

## Data assimilation for continuous global assessment of severe conditions over terrestrial surfaces

Clément Albergel<sup>1</sup>, Yongjun Zheng<sup>1</sup>, Bertrand Bonan<sup>1</sup>, Emanuel Dutra<sup>2</sup>, Nemesio Rodríguez-Fernández<sup>3</sup>, Simon Munier<sup>1</sup>, Clara Draper<sup>4</sup>, Patricia de Rosnay<sup>5</sup>, Joaquin Muñoz-Sabater<sup>5</sup>,  
5 Gianpaolo Balsamo<sup>5</sup>, David Fairbairn<sup>5</sup>, Catherine Meurey<sup>1</sup>, Jean-Christophe Calvet<sup>1</sup>

<sup>1</sup> CNRM, Université de Toulouse, Météo-France, CNRS, Toulouse, France

<sup>2</sup> Instituto Dom Luiz, IDL, Faculty of Sciences, University of Lisbon, Portugal

<sup>3</sup> CESBIO, Université de Toulouse, CNRS, CNES, IRD, Toulouse, France

<sup>4</sup> CIRES/NOAA Earth System Research Laboratory, Boulder, CO, USA

10 <sup>5</sup> European Centre for Medium-Range Weather Forecasts, Shinfield Road, Reading RG2 9AX, UK

\* Correspondence: [clement.albergel@meteo.fr](mailto:clement.albergel@meteo.fr)

**Abstract**-This study demonstrates that LDAS-Monde, a global and offline Land Data Assimilation System (LDAS), that integrates satellite Earth Observations into the ISBA (Interaction between Soil  
15 Biosphere and Atmosphere) Land Surface Model (LSM), is able to detect, monitor and forecast the impact of extreme weather on land surface states. LDAS-Monde jointly assimilates satellite derived Earth observations of surface soil moisture (SSM) and Leaf Area Index (LAI). It is run at global scale forced by the latest atmospheric reanalysis from the European Centre for Medium Range Weather Forecast (ECMWF), ERA5 (ECMWF fifth global Re Analysis, LDAS\_ERA5 hereafter)  
20 over 2010-2018 leading to a 9-yr,  $\sim 0.25^\circ \times 0.25^\circ$  spatial resolution reanalysis of Land Surface Variables (LSVs). This reanalysis is then used to compute anomalies of land surface states, in order to (i) detect regions exposed to extreme weather such as droughts and heatwave events and (ii) address specific monitoring and forecasting requirements of LSVs for those regions. In this study, LDAS\_ERA5 analysis is first evaluated worldwide using several satellite-based datasets (SSM, LAI, evapotranspiration, Gross Primary Production and Sun Induced Fluorescence), as well as in  
25 situ measurements (SSM, evapotranspiration and river discharge). The added value of assimilating the soil moisture and LAI is demonstrated with respect to a model simulation (open-loop, with no assimilation). Since the global LDAS\_ERA5 has relatively coarse resolution, two higher spatial resolution experiments over two areas particularly affected by heatwave and/or droughts in 2018  
30 were run: North Western Europe and the Murray-Darling basin in South Eastern Australia. These experiments were forced with ECMWF Integrated Forecasting System (IFS) high resolution operational analysis (LDAS\_HRES,  $\sim 0.10^\circ \times 0.10^\circ$  spatial resolution) over 2017-2018, and both open-loop and analysis experiments compared once again. Since the IFS is a forecast system, it also allows LDAS-Monde to be used in forecast mode, and we demonstrate the added value of

35 initializing 4- and 8-day LDAS\_HRES forecasts of the LSVs, from the LDAS\_HRES assimilation  
run, compared to the open-loop experiments. This is particularly true for LAI that evolves on longer  
time space than SSM and is more sensitive to initial conditions than to atmospheric forcing, even at  
an 8-day lead time. This confirms that slowly evolving land initial conditions are paramount for  
forecasting LSVs and that LDAS-systems should jointly analyse both soil moisture and vegetation  
40 states. Finally evaluation of the modelled snowpack is presented and the perspectives for snow data  
assimilation in LDAS-Monde are discussed.

## 1 Introduction

Extreme weather and climate events like heatwaves and droughts are likely to increase in frequency  
and/or magnitude (IPCC, 2012, Ionita et al., 2017). Amongst all the natural disasters, droughts are  
45 the most detrimental (Bruce, 1994; Obasi, 1994; Cook et al., 2007; Mishra and Singh, 2010; WMO  
2017) and about one-fifth of damages caused by natural hazards can be attributed to droughts  
(Wilhite 2000). They also cost society billions of dollars every year (WMO 2017). It is therefore of  
paramount importance to implement tools that can monitor and warn about drought conditions  
(Svoboda, 2002; Luo and Wood, 2007; Blyverket et al., 2019) as well as their impact on land  
50 surface variables (LSVs) and society (Di Napoli et al., 2019). A major scientific challenge in  
relation to the adaptation to climate change is to observe and simulate how land biophysical  
variables respond to those extreme events (IPCC, 2012).

Droughts can be described as a deficit of water caused by a lack of precipitation. The concept of  
drought is broad and they are generally classified according to which part of the hydrological cycle  
55 suffers from a water deficit (IPCC, 2014; Barella-Ortiz and Quintana-Seguí, 2018). Drought types  
are all related to precipitation deficit and they have severe impacts in regions with rain-fed crops  
and no irrigation. They include meteorological droughts (lack of precipitation), agricultural  
droughts (deficit of water in the soil), hydrological droughts (deficit of streamflow, water level in  
rivers) and environmental droughts (a combination of the previous droughts types). Because of the  
60 effect of precipitation deficit propagating through the whole hydrological system, it can be stated  
that all drought types are related (Wilhite, 2000). Complex interactions between continental surface  
and atmospheric processes have to be combined with human action in order to fully understand the  
wide ranging impacts of droughts on land surface conditions (Van Loon, 2015). As a consequence,  
Land Surface Models (LSMs) driven by high-quality gridded atmospheric variables and coupled to  
65 river-routing system are key tools to address these challenges (Dirmeyer et al., 2006; Schellekens et  
al., 2017). Initially developed to provide boundary conditions to atmospheric models, the role of  
LSMs has evolved and they can now be used to monitor and forecast land surface conditions

(Balsamo et al., 2015; Balsamo et al., 2018; Schellekens et al., 2017). Additionally, the representation of LSVs by LSMs can be improved through the integration of Earth Observations (EOs) (e.g. Reichle et al., 2007; Lahoz and de Lannoy, 2014; Kumar et al., 2018; Albergel et al., 2017, 2018a, 2019; Balsamo et al., 2018) as well as by coupling them with other models of the Earth system like atmosphere, oceans, river routing systems (e.g., de Rosnay et al., 2013, 2014; Kumar et al., 2018, Balsamo et al., 2018; Rodríguez-Fernández et al., 2019; Muñoz-Sabater et al., 2019). Satellite products are particularly relevant for such application. Satellite EOs related to the terrestrial hydrological, vegetation and energy cycles are now available at a global scale with high spatial resolution (at kilometric scale and below) and with long-term records (e.g., Lettenmaier et al., 2015, Balsamo et al., 2018). Combining EOs and LSMs through Land Data Assimilation Systems (LDASs) could lead to enhanced initial land surface conditions which, in turn, lead to improved forecasts of weather patterns, sub-seasonal temperature and precipitation, agricultural and vegetation productivity, seasonal streamflow, floods and droughts, as well as the carbon cycle (Banzai and Shukla, 1999; Schlosser and Dirmeyer, 2001; Bierkens, M. and van Beek, 2009; Koster et al., 2010; Bauer et al., 2015; Massari et al., 2018; Albergel et al., 2018a, 2019, Rodríguez-Fernández et al., 2019; Muñoz-Sabater et al., 2019). Amongst the current land-only LDAS activities several are NASA-led (National Aeronautics and Space Administration) projects. Examples of such activities are the Global Land Data Assimilation System (GLDAS, Rodell et al., 2004) which is run at a global scale. While the North American Land Data Assimilation System (NLDAS, Xia et al., 2012a, b) and the National Climate Assessment-Land Data Assimilation System (NCA-LDAS, Kumar et al., 2016, 2018, 2019) are run over the continental United States of America and the Famine Early Warning Systems Network (FEWS NET) Land Data Assimilation System (FLDAS, McNally et al., 2017) is run e.g. over Western, Eastern and Southern Africa. Finally, the Carbon Cycle Data Assimilation System (CCDAS, Kaminski et al., 2002), the Coupled Land Vegetation LDAS (CLVLDAS, Sawada and Koike, 2014, Sawada et al., 2015), the Data Assimilation System for Land Surface Models using CLM4.5 proposed by Fox et al., 2018, the SMAP (Soil Moisture Active Passive) level 4 system (Reichle et al., 2019) as well as LDAS-Monde (Albergel et al., 2017, 2018, 2019) developed by the research department of Météo-France are additional initiatives of combining EOs and LSMs through data assimilation. Few studies have, however, included the assimilation of multiple EOs and considered global applications (Kumar et al., 2018, Albergel et al., 2019). A more detailed description of the various existing LDASs is available in Kumar et al., 2018, Albergel et al., 2019 and references therein.

After several applications at regional and continental scales (Albergel et al., 2017, 2018, 2019, Leroux et al., 2018, Tall et al., 2019, Blyverket et al., 2019, Bonan et al., 2019), LDAS-Monde was

run at global scale forced by the latest atmospheric reanalysis from the European Centre for Medium Range Weather Forecast (ECMWF), ERA5, over 2010-2018 leading to a 9-yr, 0.25° x 0.25° spatial resolution reanalysis of the LSVs (LDAS\_ERA5). In this study, stemming from  
105 previous works referenced above, it is shown that LDAS-Monde global, offline, joint integration of Surface Soil Moisture (SSM) and Leaf Area Index (LAI) EOs into the ISBA (Interaction between Soil Biosphere and Atmosphere) LSM (Noilhan and Planton, 1989, Noilhan and Mahfouf, 1996) can be used to detect, monitor and forecast the impact of extreme events on LSVs. Are presented in this study:

110 • An evaluation at global scale using diverse and complementary datasets such as evapotranspiration from the GLEAM project (Miralles et al., 2011, Martens et al., 2017), Gross Primary Production (GPP) from the FLUXCOM project (Tramontana et al., 2016, Jung et al., 2017), Solar Induced Fluorescence (SIF) from the GOME-2 (Global Ozone Monitoring Experiment-2) scanning spectrometer (Munro et al., 2006, Joiner et al., 2016) and snow cover data  
115 from the Interactive Multi-sensor Snow and Ice Mapping System (or IMS, <https://www.natice.noaa.gov/ims/>, last accessed June 2019). It is also validated using reference observations including in situ evapotranspiration from the FLUXNET 2015 synthesis data set (<http://fluxnet.fluxdata.org/>, last accessed June 2019), soil moisture from the International Soil Moisture Network (ISMN, <https://ismn.geo.tuwien.ac.at/en/>, last accessed June 2019) as well as  
120 river discharge from several networks across the world.

• An estimation of the mean LSVs climate over 2010-2018, used as reference for computing anomalies of the land surface conditions to (i) detect regions exposed to extreme weather such as drought and heatwave events in 2018 and (ii) trigger more detailed monitoring and forecasting activities of the LSVs for those regions at higher spatial resolution.

125 The paper is organised in four sections as it follows: section 2 details the various components constituting LDAS-Monde: the ISBA LSM, the data assimilation scheme and the EOs assimilated as well as the different atmospheric forcing datasets used, followed by the experimental and evaluation setup. Section 3 describes and discusses the impact of the analysis on the representation of the LSVs. The selection of 2 case studies over regions particularly affected by extreme events  
130 during 2018 and their detailed monitoring at higher spatial resolution combined with land surface forecasting activities is also presented. Finally section 4 provides conclusions and prospects for future work.

## 2 Material and methods

The following subsections briefly describe the main components of LDAS-Monde: the ISBA  
135 LSM, its data assimilation scheme and two other key elements of the setup: atmospheric forcing  
and assimilated satellite derived observations. The experimental setup and the evaluation datasets  
used in this study are also presented.

## 2.1 LDAS-Monde

### 2.1.1 ISBA Land Surface Model

140 Embedded within the SURFEX (SURFace EXternalisée, Masson et al., 2013, version 8.1)  
modelling platform developed by the research department of Météo-France (CNRM, Centre  
National de Recherches Météorologiques), LDAS-Monde (Albergel et al., 2017) allows the joint  
integration of satellite derived SSM and LAI into the CO<sub>2</sub>-responsive (Calvet, et al., 1998, 2004,  
Gibelin et al., 2006), multilayer diffusion scheme (Boone et al., 2000, Decharme et al., 2011)  
145 version of the ISBA LSM (Noilhan and Planton, 1989, Noilhan and Mahfouf, 1996) using a  
simplified version of an Extended Kalman Filter (SEKF, e.g. Mahfouf et al., 2009, Barbu et al.,  
2011, Fairbairn et al., 2017). It can be coupled to the ISBA-CTRIIP hydrological model (ISBA-  
CTRIIP for ISBA-CNRM, Total Runoff Integrating Pathways) as detailed in Decharme et al., (2019).  
In such a configuration, ISBA is able to represent the transfer of water and heat through the soil  
150 based on a multilayer diffusion scheme, as well as plant growth and leaf-scale physiological  
processes. ISBA models key vegetation variables like LAI and above ground biomass, the diurnal  
cycle of water, carbon and energy fluxes. It computes a soil-vegetation composite using a single-  
source energy budget. In the CO<sub>2</sub>-responsive versions of ISBA, ISBA-A-gs, the model can simulate  
the CO<sub>2</sub> net assimilation and GPP by considering the functional relationship between the  
155 photosynthesis rate (A) and the stomatal aperture (gs) based on the biochemical A-gs model  
proposed by Jacob et al., 1996. Photosynthesis is in control of the evolution of vegetation variables.  
It makes vegetation growth possible as a result of an uptake of CO<sub>2</sub>. Oppositely, a deficit of  
photosynthesis triggers higher mortality rates. Ecosystem respiration (RECO) is represented by the  
CO<sub>2</sub> being released by the soil-plant system and GPP by the carbon uptake related to  
160 photosynthesis. Finally, the net ecosystem exchange (NEE) consists of the difference between GPP  
and RECO. Each ISBA grid cell can be composed of up to 12 generic land surface types, bare soil,  
rocks, and permanent snow and ice surfaces as well as nine plant functional types (needle leaf trees,  
evergreen broadleaf trees, deciduous broadleaf trees, C3 crops, C4 crops, C4 irrigated crops,  
herbaceous, tropical herbaceous and wetlands). The ECOCLIMAP-II land cover database (Faroux  
165 et al., 2013) provides ISBA parameters for all of them.

ISBA multilayer diffusion scheme's default discretization is 14 layers over 12 m depth. The following configuration is used in this study: thickness (depth) of each layers are (from top to bottom), 1 cm (0-1 cm), 3 cm (1-4 cm), 6 cm (4-10 cm), 10 cm (10-20 cm), 20 cm (20-40 cm), 20 cm (40-60 cm), 20 cm (60-80 cm), 20 cm (80-100 cm), 50 cm (100-150cm), 50 cm (150-200cm), 100 cm (200-300 cm), 200 cm (300-500 cm), 300 cm (500-800 cm) and 400 cm (800 to 1200 cm), see also Figure 1 of Decharme et al., 2011. Snow is represented using the ISBA 12-layers explicit snow scheme (Boone and Etchevers, 2001, Decharme et al., 2016).

### 2.1.2 CTRIP river routing system

The ISBA-TRIP river routing system is able to simulate continental scale hydrological variables based on a set of three prognostic equations. They correspond to (i) the groundwater, (ii) the surface stream water and (iii) the seasonal floodplains. It converts the runoff simulated by ISBA into river discharge. ISBA-CTRIP river-routing network has a spatial resolution of  $0.5^\circ \times 0.5^\circ$  globally and is coupled daily with ISBA through the OASIS3-LCT coupler (Voldoire et al., 2017). ISBA provides to CTRIP updated fields of runoff, drainage, groundwater and floodplain recharges. In turn, CTRIP provides ISBA with water table depth, floodplain fraction as well as flood potential infiltration so that ISBA can simulate capillarity rise, evaporation and infiltration over flooded areas. A comprehensive overview of ISBA-CTRIP is available in Decharme et al., (2019).

### 2.1.3 Data assimilation

The SEKF used in LDAS-Monde is a 2-step sequential approach in which a forecast step is followed by an analysis step. The forecast step propagates the initial state of the model (being a short term forecast from the ISBA LSM) and then, the analysis step corrects this forecast by assimilating observations. The flow-dependency (dynamic link) between the prognostic variables and the observations is ensured in the SEKF through the observation operator Jacobians, which propagate information from the observations to the analysis via finite-difference computations (de Rosnay et al., 2013). The analysis involves the computation of a Jacobian matrix having as many rows as assimilated observation types (here two: SSM and LAI) and as many columns as model control variables requested (here eight soil layer, 1-100cm, and LAI). In addition to a control run, computing the Jacobian matrix requires perturbed runs, one for each control variable. The eight control variables are directly updated using their sensitivity to observed variables (i.e. defined by the Jacobians). Other variables are indirectly modified through biophysical processes and feedbacks from the model. Several studies (e.g. Draper et al., 2009; Rüdiger et al., 2010) have demonstrated that small perturbations lead to a good approximation of this linear behaviour, provided that computational round-off error is not significant. Typically, for those runs, the initial state of the control variable is perturbed by about 0.1% (see Albergel et al., 2017; Rüdiger et al., 2010). The

200 length of the LDAS-Monde assimilation window is 24-hours. A mean volumetric standard deviation error is specified proportional to the soil moisture range (the difference between the volumetric field capacity and the wilting point, calculated as a function of the soil type, as given by Noilhan et Mahfouf, 1996) and scaled by a factor 0.04 for SSM in its model equivalent (the second layer of soil between 1 and 4 cm), scaled with and 0.02 for deeper layers (soil layer 3 to 8, 4-100cm). The  
205 observational SSM error follows the same rule scaled by 0.05 and is consistent with errors typically expected for remotely sensed SSM (e.g., de Jeu et al., 2008, Gruber et al, 2016). Soil moisture errors for both the model and the observations are assumed to be proportional to the soil moisture range (being defined as the difference between the volumetric field capacity and the wilting point, calculated as a function of the soil type, as given by Noilhan et Mahfouf, 1996). Based on previous  
210 results from Jarlan et al., 2008, Rüdiger et al., 2010, Barbu et al., 2011, observed and modelled LAI standard deviation errors are set to 20 % of the LAI value itself for values higher than  $2\text{m}^2\text{m}^{-2}$ . For LAI values lower than  $2\text{m}^2\text{m}^{-2}$ , a fixed value of  $0.04\text{m}^2\text{m}^{-2}$  has been used. More detailed can be found in Barbu et al., 2011 (section 2.3 on data assimilation scheme and figure 2).

## 2.2 Atmospheric forcing

215 The lowest model level (about 10-meters above ground level) of air temperature, wind speed, specific humidity and pressure and the downwelling fluxes of shortwave, longwave radiations as well as precipitation (partitioned in solid and liquid phases) are needed to force LDAS-Monde. In this study, LDAS-Monde is driven by several near-surface meteorological fields from ECMWF, its most recent atmospheric reanalysis (ERA5), or its high resolution operational weather analysis and  
220 forecasts (HRES). ERA5 (Hersbach et al., 2018, 2019 submitted) is the fifth generation of global reanalyses produced by ECWMF. This atmospheric reanalysis is a key element of the Copernicus Climate Change Service (C3S) and is available from 1979 onward (data is released about 2 months behind real time). ERA5 has hourly output analysis, 31 km horizontal dimension and 137 levels in the vertical resolution. Several studies have validated the ERA5 datasets, for example Urraca et al.  
225 (2018) have compared incoming solar radiation from both ERA5 and the ERA-interim reanalysis (Dee et al., 2011) at a global scale and found evidence that ERA5 outperforms ERA-Interim. In another study, Beck et al. (2019) have highlighted the good performance of ERA5 precipitation with respect to a set of 26 gridded (sub-daily) precipitation data sources by comparing them to Stage-IV gauge-radar data over the CONUS domain (CONTinental United States of America). Tall et al.  
230 (2019) have used in situ measurements of precipitation at more than 100 stations spanning all over Burkina-Faso in western Africa as well as incoming solar radiation from 4 in situ stations to evaluate the quality of ERA5 over ERA-Interim also with positive outcomes for ERA5 as well.

They have also evaluated both reanalysis datasets through their impact on the representation of LSVs when used to force the ISBA LSM, again demonstrating a clear advantage for ERA5. Similar work has been done by Albergel et al. (2018a), over North America, this study found enhanced performances in the representation of evaporation, snow depth, soil moisture as well as river discharge when the ISBA LSM was forced by ERA5 compared to ERA-Interim. At the time of the study, ERA5 underlying model and data assimilation system (Cycle 41r2) are very similar to that of the operational weather forecast, HRES, which has production cycles ranging from 41r2 to 45r1 during the study period(it is 46r1 from June 2019, more information at <https://www.ecmwf.int/en/forecasts/documentation-and-support/changes-ecmwf-model>, last accessed July 2019). The main difference between ERA5 and HRES over the considered period is the horizontal resolution, 9 km in HRES and 31 km in ERA5. The atmospheric forcing is interpolated from the native grids of ERA5 and HRES to regular grids of  $0.25^\circ \times 0.25^\circ$  and  $0.1^\circ \times 0.1^\circ$ , respectively, using a bilinear interpolation from the native grid to the regular grid. The four neighbouring cells in the source grid fitting latitude and longitude were linearly interpolated. ERA5 and HRES were used in Albergel et al. (2019) to force LDAS-Monde in order to study the impact of the 2018 summer heatwave in Europe. Authors have highlighted that the HRES configuration exhibits better monitoring skills than the coarser resolution ERA5 configuration.

From the forecast initialized at 00:00 UTC, HRES is also available with a 10-day lead time, but with changes in the temporal resolution. HRES forecast step frequency is hourly up to time step 90 (i.e. day 3), 3-hourly from time-step 90 to 144 (i.e. day 6) and 6-hourly from time-step 144 to 240 (i.e. day 10). In this study, for forecast experiments (see section 2.4 for details on the experimental setup) HRES forecasts with a 10-day lead time are used to initialize forecasts of the LSVs from LDAS\_HRES open-loop and analysis configurations in order to evaluate the impact of the initialisation on the forecast of LSVs. The original 3-hourly time steps are used up to day 6 (time step 144), the 6-hourly time steps from day 6 to 10 are interpolated to 3-hourly frequency to avoid discontinuities.

### 2.3 Assimilated satellite Earth Observations

Two types of satellite derived variables are assimilated in LDAS-Monde, ASCAT Soil Water Index (SWI) and LAI GEOV1. They are both freely available through the Copernicus Global Land Service (CGLS, <https://land.copernicus.eu/global/index.html>, last accessed June 2019). They are illustrated by Figure 1.

ASCAT stands for Advanced Scatterometer, it is an active C-band microwave sensor that is onboard the European MetOp polar orbiting satellites (METOP-A, from 2006, B from 2012 and also C from



2018). From ASCAT radar backscatter coefficients, it is possible to derive information on SSM following a change detection approach (Wagner et al., 1999, Bartalis et al., 2007). The recursive form of an exponential filter (Albergel et al., 2008), is then applied to estimate the SWI using a timescale parameter, T (varying between 1 day and 100 days) and ranging between 0 (dry) and 100 (wet). T is a surrogate parameter for all the processes potentially affecting the temporal dynamics of soil moisture (like, soil hydraulic properties and thickness of the soil layer, evaporation, run-off and vertical gradient of soil properties such as texture and density). In this study, CGLS SWI-001 (i.e. produced with a T-value of 1 day) is used as a proxy of SSM (Kidd et al., 2013). Grid points with an average altitude exceeding 1500 m above sea level as well as those with more than 15 % of urban land cover were rejected as those conditions are known to affect the retrieval of SSM. Prior to the assimilation, SSM has to be converted from the observation space to the model space. This is done through a linear rescaling as proposed by Scipal et al. (2007), where the mean and variance of observations are matched to the mean and variance of the modelled soil moisture from the second layer of soil (1-4 cm depth). This rescaling gives in practice very similar results to CDF (cumulative distribution function) matching. The linear rescaling is performed on a seasonal basis (with a 3-month moving window) as suggested by Draper et al., (2011), Barbu et al., (2014). As in Albergel et al., 2018a, 2018b, pixels whose average altitude exceeds 1500 m above sea level as well as pixels with urban land cover fractions larger than 15% were discarded as those conditions may affect the retrieval of soil moisture from space.

285 The LAI GEOV1 observations are based on data from from both SPOT-VGT and then PROBA-V satellites. They span from 1999 to present, have a 1km x 1km spatial resolution and are produced daily according to the methodology developed by Baret et al. (2013). As in previous studies (e.g, Barbu et al., 2014, Albergel et al., 2019), observations are interpolated by an arithmetic average to the model grid points ( $0.25^\circ$  or  $0.10^\circ$  in this study), if at least 50 % of the model grid points are observed (i.e. half the maximum amount). LAI GEOV1 observations have a temporal frequency of 10 days at best (in the presence of clouds, no observation are available). LAI data are masked in the presence of snow from the open-loop experiment.

## 2.4 Experimental setup

295 LDAS-Monde is first run at a global scale, at  $0.25^\circ \times 0.25^\circ$  spatial resolution, forced by ERA5 atmospheric reanalysis and assimilating SSM and LAI EOs from 2010 to 2018 (LDAS\_ERA5 hereafter). LDAS-ERA5 was spun-up by running year 2010 twenty times. LDAS\_ERA5 analysis as well as its model counterpart (open-loop, i.e. no data assimilation) are presented and evaluated in this study.

This 9-yr global reanalysis was then used to provide a monthly climatology for estimating anomalies of the land surface conditions. For each month (and variable considered) of 2018 we have removed the monthly mean and scaled by the monthly standard deviation of the 2010-2018 period. Significant anomalies were used to trigger more detailed monitoring as well as forecasting activities for a region of interest. 19 regions across the globe known for being potential hot spots for droughts and heat waves were selected. They are listed in Table I and presented in Figure 2. Monthly anomalies of LDAS\_ERA5 analysis of SSM and LAI for those 19 regions are assessed for 2018 (with respect to the 2010-2018 period) and regions presenting significant level of anomalies were selected and further investigated. For those region, LDAS-Monde has been driven by HRES atmospheric analysis leading to a  $0.1^\circ \times 0.1^\circ$  reanalysis of the LSVs from April 2016 to December 2018 (LDAS\_HRES hereafter). HRES is available at a  $0.1^\circ \times 0.1^\circ$  resolution only from April 2016. April to December 2016 is used as a short period for spin-up and results are presented for the period 2017-2018. Although a 9-month spin-up period can be seen as rather short, evaluating LDAS-HRES on either 2017-2018 or 2018 (using instead a 21-month spin-up) leads to similar results on surface soil moisture and LAI (not shown). While the system is not fully spun-up, it can be considered as representative of the system response to data assimilation. LDAS\_HRES complements the coarser spatial resolution LDAS\_ERA5. HRES forecasts with a 10 day lead time are also used, and initialised by either LDAS\_HRES open-loop or analysis (LDAS\_Fc hereafter) in order to assess the impact of the initialisation on the forecast. A summary of the experimental setup is given in Table II.

## 2.5 Evaluation datasets and metrics

This study uses several satellite-derived estimates of EOs as well as in situ measurement data. LDAS\_ERA5 analysis impact is assessed with respect to the open-loop model run (i.e. no assimilation). The two assimilated datasets, CGLS SSM and LAI, were used to verify to which extent the assimilation system was able to correctly integrate them (i.e. suggesting a healthy behaviour from the data assimilation system). Then several spatially distributed datasets independent from both experiments: (namely) evapotranspiration from the GLEAM project (Miralles et al., 2011, Martens et al., 2017, version 3b entirely satellite driven), Gross Primary Production (GPP) from the FLUXCOM project (Tramontana et al., 2016, Jung et al., 2017), Sun Induced Fluorescence (SIF) from the GOME-2 (Global Ozone Monitoring Experiment-2) scanning spectrometer (Munro et al., 2006, Joiner et al., 2016) and snow cover data from the Interactive Multi-sensor Snow and Ice Mapping System (or IMS, <https://www.natice.noaa.gov/ims/>) were used in the evaluation process. The IMS snow cover product combines ground observations and satellite

data from microwave and visible sensors (using geostationary and polar orbiting satellites) to provide snow cover information in all weather conditions. The IMS product is available daily for the northern hemisphere.

335 In situ measurements of surface soil moisture from 19 networks across 14 countries available from the ISMN are also used to evaluate the performance of the soil moisture analysis. They represent 782 stations with at least 2 years of daily data over 2010-2018. Sensors at 5 cm depth (SSM) are compared with soil moisture from LDAS\_ERA5 third layer of soil (4-10 cm), sensors a 20 cm with the forth layer of soil (10-20 cm, 685 stations from 10 networks). Beside 11 stations located in 4  
340 countries of Western Africa (Benin, Mali, Sénégal and Niger) and 21 stations in Australia, most of the station are located in North America and Europe, see Table S3.

Most of these ground stations for all types of in situ observations are located in Europe and North America and they have been used in previous studies (e.g. Albergel et al., 2017, 2018a,b, Leroux et al., 2018) to assess the LDAS-Monde quality. Therefore, the LDAS-Monde evaluation using ground  
345 measurements is discussed in the result section while figures are reported as supplementary materials of this study. Evaluation datasets are listed in Table III along with the metrics used (correlation, Root Mean Square Differences -RMSD- and unbiased RMSD -ubRMSD- and bias). For in situ datasets, a Normalized Information Contribution (NIC, Eq.(1)) measure is applied to the correlation values to quantify the improvement or degradation due to the specific configuration. For  
350 global estimates, Normalized RMSD ( $N_{RMSD}$ , Eq.(2)) was used, also. Finally, for surface soil moisture, R was calculated for both absolute and anomaly time-series in order to remove the strong impact from the SSM seasonal cycle on this specific metric (see e.g. Albergel et al., 2018a, 2018b).

$$NIC_R = \frac{R_{[Analysis]} - R_{[Model]}}{1 - R_{[Model]}} \times 100 \quad \text{Eq.(1)}$$

$$N_{RMSD} = \frac{RMSD_{[Analysis]} - RMSD_{[Model]}}{RMSD_{[Model]}} \times 100 \quad \text{Eq.(2)}$$

355 NIC scores were classified according to three categories: (i) negative impact from the analysis with respect to the open-loop with values smaller than -3 %, (ii) positive impact from the analysis with respect to the open-loop with values greater than +3 % and (iii) neutral impact from the analysis with respect to the open-loop with values between -3 % and 3 %.

The Nash-Sutcliffe Efficiency score (NSE, Eq.(3), Nash and Sutcliffe, 1970) is used to evaluate  
360 LDAS\_ERA5 experiments ability to represent the monthly discharge dynamics.

$$\text{NSE} = 1 - \frac{\sum_{mt=1}^T (Q_s^{mt} - Q_o^{mt})^2}{\sum_{mt=1}^t (Q_s^{mt} - \overline{Q_s^{mt}})^2} \quad \text{Eq.(3)}$$

where  $Q_s^{mt}$  is the monthly river discharge from LDAS\_ERA5 (analysis or open-loop) at month  $mt$ , and  $Q_o^{mt}$  is the observed river discharge at month  $mt$ . NSE can vary between  $-\infty$  and 1. An exact match between model predictions and observed data is defined as a value of 1, whereas a value of 0 means that the model predictions have the same accuracy as the mean of the observed data. Finally negative values represent when the observed mean is a better predictor than the model simulation. NIC presented in Eq.(1) has also been applied to NSE scores to assess the added value of LDAS\_ERA5 analysis over its open-loop counterpart. Stations with NSE values lesser that -2 were discarded. Similar threshold has already been used in previous studies evaluating LDAS-Monde (e.g. Albergel et al., 2017, 2018a). Many processes, most of them linked to water management such as the presence of dams and reservoirs, irrigation, water uptake in urban areas, are not yet represented in ISBA possibly leading to a poor representation of river discharges. As previous evaluations studies have suggested a neutral to positive impact from the assimilation, only, it has been decided to focus on stations with reasonable NSE values.

As for SIF, in ISBA the fluorescence is not simulated directly, however photosynthesis activity is simulated through the calculation of the GPP, which is driven by plant growth and mortality in the model. Modelled GPP values are expressed in  $\text{g(C)} \cdot \text{m}^{-2} \cdot \text{day}^{-1}$ , while SIF is an energy flux emitted by the vegetation ( $\text{mW} \cdot \text{m}^{-2} \cdot \text{sr}^{-1} \cdot \text{nm}^{-1}$ ). Hence, GPP and SIF cannot be directly compared as they do not represent the same physical quantities. However, several studies (e.g, Zhang et al., 2016, Sun et al., 2017, Leroux et al., 2018) have found that their time dynamics investigated, highlighting the potential of SIF products to be used as a validation support for GPP models.

### 3 Results

#### 3.1 Global assessment of LDAS\_ERA5

##### 3.1.1 Gridded datasets

Figure 3 presents mean RMSD values between the observations and LDAS\_ERA5 for the open-loop (Figure 3a), and for the analysis (Figure 3b) for LAI over 2010-2018. Because LAI observations are ingested into the model, the assimilation reduces the LAI RMSD values almost everywhere. It can be noted that rather large LAI RMSD values ( $> 1.5 \text{ m}^2\text{m}^{-2}$ ) can remain in some areas after the assimilation, especially in densely forested areas. Figure 4 illustrates latitudinal plots

390 of LAI, SSM, GPP and evapotranspiration for LDAS\_ERA5 before assimilation (the open-loop) and after assimilation (the analysis) along with observations. The number of points considered per latitudinal stripes of  $0.25^\circ$  is represented, also. From Figure 4a it is possible to see the positive impact of the analysis compared to the open-loop, with the former being closer to the observations. Improvement from the analysis occurs from nearly  $80^\circ$ North to about  $55^\circ$  South, areas around the equator are particularly improved. A smaller impact than for LAI is obtained for SSM, GPP and EVAP, hardly visible at this scale. The mean latitudinal results show a consistent difference in terms of GPP and Evapotranspiration between the LDAS\_ERA5 and the observational products. These differences are systematic with higher values in tropical regions. Figure 5 represents latitudinal plots of score differences (correlations and normalized RMSD) for LAI, SSM, GPP, EVAP and SIF (Figure 5i, correlation only). Score differences are computed as follow, analysis minus open-loop using monthly averages over 2010-2018 for LAI and SSM, 2010-2013 for GPP, 2010-2016 for EVAP and 2010-2015 for SIF. For SIF only differences in correlation are represented as it is used to evaluate GPP variability as in Leroux et al., 2018. For each panel of Figure 5, the vertical dashed line represents the 0-value. Therefore, for plots of correlation differences, positive values indicate an improvement from the analysis with respect to the open-loop simulation. Similarly, for plots of RMSD differences negative values indicate an improvement from the analysis with respect to the open-loop simulation. LAI and SSM being assimilated variables, the analysis leads to a clear improvement in both correlation and RMSD. Such improvement is expected and reflects the healthy behaviour of the assimilation system. Both variables are improved at almost all latitudes with the exception around  $45^\circ$ S for LAI correlation values (very few land points). For SSM a noticeable improvement in both correlation and RMSD is found around  $20^\circ$ N corresponding mainly to an improvement in the Sahara desert (not shown). Being linked to LAI, GPP is also improved across almost all latitudes (to a lesser extend than LAI) with a particularly positive impact below  $20^\circ$ N. As seen on Figure 5 d) and i), there is little impact on variable EVAP which can be considered negligible. It highlights the difficulty of land surface data assimilation to impact model fluxes by modifying model states. Panels of Figure 6 illustrate histograms of score differences (correlation and RMSD, analysis minus open-loop) for LAI, SSM, GPP, EVAP and SIF. The Number of available data as well as the percentage of positive and negative values are reported. For correlations ( $N_{\text{RMSD}}$ ) differences, positive (negative) values indicate an improvement from the analysis over the open-loop. It complements Figure 5. Regarding LAI the analysis improves 96.9% of the grid points for correlations and 99.9% for  $N_{\text{RMSD}}$ . As for SSM, correlation values are improved for 92.8% of the grid points, it is 92.4% for  $R_{\text{MSD}}$ . When using independent datasets such as GPP and SIF, one may also notice an improvement from the analysis, correlation ( $N_{\text{RMSD}}$ ) are

425 better for 81.1% (74.1%), 79.7% (SIF  $N_{\text{RMSD}}$  N/A) of the grid points. Results using the GLEAM dataset for evapotranspiration are more contrasted with 63.6% (48.9%) of the grid points showing an improvement from the analysis and it is worth mentioning that 24.9% (39.6%) of the grid point shows a decrease in skill. However GLEAM is an evaporation model designed to be driven by remote sensing observations only. GLEAM only estimates (root-zone) soil moisture and terrestrial evaporation while the CO<sub>2</sub>-responsive version of ISBA in LDAS\_ERA5 is a physically-based land surface model, accounting for more processes linked to vegetation (see section 2.1.1). It has to be noted that the auxiliary dataset used to e.g. represent the different land cover types are different also. Within GLEAM, the land cover types fractions are sourced from the Global Vegetation Continuous Fields product (MOD44B), based on observations from the Moderate Resolution Image Spectroradiometer (MODIS). Four land cover types are considered, bare soil, low vegetation (e.g. grass), tall vegetation (e.g. trees), and openwater (e.g. lakes). In ISBA the 12 land cover types fraction depart from prevalent land cover products such as CLC2000 (Corine Land Cover) and GLC2000 (Global Land Cover). It can potentially impact the distribution of the terrestrial evaporation between GLEAM and ISBA. Further work at CNRM will focus on understanding the differences between ISBA and GLEAM, in particular investigating the sub-components of 440 terrestrial evaporation.

Finally, Figure S1 and Figure S2 illustrate snow cover evaluation. LDAS\_ERA5 snow cover was evaluated against the IMS snow cover (as e.g. in Orsolini et al., 2019). Figure S1 shows the averaged northern hemisphere snow cover fraction for the 2010-2018 period. It is complemented by all panels of Figure S2 showing (i) maps of IMS snow cover (top row) for 3 seasons, September-October-November (SON), December-January-February (DJF) and March-April-May (MAM), 445 respectively, (ii) maps of snow cover from LDAS\_ERA5 open-loop (second row), (iii) maps of snow cover differences between the open-loop and IMS data and (iv) maps of snow cover differences between the analysis and the open-loop. LDAS\_ERA5 open-loop compares very well with the IMS snow-cover data in the accumulation season from September to February (Figure S2 and panels d) to I) of Figure S1), only with an overestimation over the Tibetan Plateau. The issue over Tibet from ERA5 is not new, and consistent with previous studies like Orsolini et al., 2019. An early melt in spring compared to observations is noted in LDAS\_ERA5 and could be related with the snow cover parametrization in ISBA. As expected, the analysis has an almost neutral impact on snow as both SSM and LAI observations are filtered out from frozen/snow condition and as there is 450 no snow data assimilation in LDAS\_ERA5 (Figure S2 and panels (j), (k) and (l) of Figure S1). This clearly shows, however an area of potential improvement of data assimilation within LDAS-Monde using satellite data such as the IMS one (as in e.g. de Rosnay et al., 2014).

### 3.1.2 Ground-based datasets

LDAS\_ERA5 analysis and open-loop are also evaluated using in situ measurements of evapotranspiration, river discharge and surface soil moisture across the world. Daily in situ measurements of evapotranspiration from the FLUXNET-2015 synthesis data set (<http://fluxnet.fluxdata.org/>, last accessed June 2019) are first used in this study. The LDAS\_ERA5 ability to represent evapotranspiration is evaluated using correlation (R), RMSD and ubRMSD as well as bias (LDAS\_ERA5 minus observations) using the 85 selected FLUXNET-2015 stations. Median R, RMSD, ubRMSD and bias for LDAS\_ERA5 analysis (open-loop) are 0.73 (0.72), 28.74 (29.60) W.m<sup>-2</sup>, 27.37 (26.92) W.m<sup>-2</sup> and 4.64 (4.40) w.m<sup>-2</sup>, respectively. If these numbers depict a small advantage of the analysis over the open-loop configuration, it is worth mentioning that differences are rather small and likely to fall within the uncertainty of the in situ measurement.

Figure S3(a) represents the added value of the analysis based on NIC<sub>R</sub> (Eq.(1)), large blue circles represent a positive impact from the analysis (20 stations) at NIC<sub>R</sub> greater than +3 (i.e. R values are better when the analysis is used than when the model is used) while large red circles represent a degradation from the analysis (5 stations) at NIC<sub>R</sub> smaller than -3. Stations with a rather neutral impact (60 stations) at NIC<sub>R</sub> between [-3 ; +3] are not reported for sake of clarity. Figure S3 (b), (c), (d) and (e) are scatter-plots of R, ubRMSD, absolute bias and RMSD between LDAS\_ERA5 open-loop and the 85 stations from the Fluxnet2015 (y-axis) against LDAS\_ERA5 analysis and the same pool of stations (x-axis). 56 stations (out of 85) have better R values considering the analysis. They are 41 for ubRMSD, 47 for RMSD and 44 for absolute bias.

Results on river discharge are illustrated by Figures S4 and S5. Figure S4 represents NSE scores and as NSE values below -2 were discarded, it leads to a subset of 982 stations available. Most of them are located in North America and Europe while a few are available in South America and Africa. Figure S4 is complemented by Figure S5. Panel a) of Figure S5 represents the NIC scores applied to NSE scores and emphasizes the added value of LDAS\_ERA5 analysis over the open-loop. 74% of this subset of stations presents a rather neutral impact from the analysis (at NIC ranging between -3 and +3) while 26% (254 stations) presents an impact greater or smaller than 3%. When the analysis impacts the representation of river discharge, this impact tends to be positive with 74% (189 stations) having a NIC score greater than 3% while only 26% (65 stations) presents NIC score smaller than -3%. These results are supported by panels (b) and (c) of Figure S5, also (density of NSE scores for LDAS\_ERA5 analysis and open-loop, scatter-plot of NSE scores for LDAS\_ERA5 analysis and open-loop, respectively).

490 The statistical scores for soil moisture from LDAS\_ERA5 open-loop and analysis (third and fourth layers of soil, 4-10 cm depth, 10-20 cm depth, respectively) over 2010-2018 when compared with ground measurements from the ISMN (5 cm depth and 20 cm depth) are presented in Table S3 for each individual network. Averaged statistical metrics (ubRMSD, R,  $R_{\text{anomaly}}$  and bias) are similar for both LDAS\_ERA5 analysis and open-loop even if local differences exist. For the analysis, averaged  
495 R ( $R_{\text{anomaly}}$ ) values along with its 95% Confidence Interval (CI) using in situ measurements at 5 cm (782 stations from 19 networks) are  $0.68 \pm 0.03$  ( $0.53 \pm 0.04$ ) ( $0.67 \pm 0.03$  ( $0.53 \pm 0.04$ ) for the open-loop) with averaged-network values going up to  $0.88 \pm 0.01$  ( $0.58 \pm 0.04$ ) for the analysis (SOILSCAPE network, 49 stations in the USA) and always higher than 0.55 except for one network, ARM (10 stations in the USA) presenting an averaged R value of  $0.29 \pm 0.05$ . Averaged  
500 ubRMSD and bias (LDAS\_ERA5 minus in situ) are  $0.060 \text{ m}^3\text{m}^{-3}$  and  $0.077 \text{ m}^3\text{m}^{-3}$  for the analysis,  $0.060 \text{ m}^3\text{m}^{-3}$  and  $0.076 \text{ m}^3\text{m}^{-3}$  for the open-loop, respectively. NIC (Eq.1) has also been applied to R values, 65% of the pool of stations present a neutral impact from the analysis (511 stations at NIC ranging between -3 and +3), 12% present a negative impact (91 stations at NIC < -3) and 23% present a positive impact at (180 stations at NIC > +3).

505 The number of stations where R differences between the analysis and the open-loop are significant (i.e. their 95% CI are not overlapping) is 186 out of 782 (about 26%). There is an improvement from the analysis w.r.t. the open-loop for 128 stations (out of 186, i.e. about 69%) and a degradation for 58 stations (about 31%). Figure 7 illustrates R differences between the analysis and the open-loop runs. When differences (analysis minus openloop) are not significant stations are represented  
510 by a small dot. When they are significant, large circles have been used, blue for positive differences (an improvement from the analysis) and red for negative differences (a degradation from the analysis). For most of the stations where a significant difference is obtained, it represent an improvement from the analysis.

Averaged analysis R (95%CI), bias and ubRMSD for the fourth layer of soil (685 stations from 10  
515 networks) are  $0.65 \pm 0.03$ ,  $0.049 \text{ m}^3\text{m}^{-3}$  and  $0.055 \text{ m}^3\text{m}^{-3}$ , respectively. For the open-loop, they are  $0.64 \pm 0.03$ ,  $0.048 \text{ m}^3\text{m}^{-3}$  and  $0.056 \text{ m}^3\text{m}^{-3}$ , respectively. For soil moisture at that depth, about 60% of the stations present a neutral impact from the analysis (410 stations at NIC ranging between -3 and +3), 28% a positive impact (189 stations at NIC > +3) and 12% a negative impact (86 stations at NIC < -3). Although differences between the open-loop run and the analysis are rather small, these  
520 results underline the added value of the analysis with respect to the model run. Figure S6 represents the distribution of the scores values for LDAS\_ERA5 open-loop and analysis using boxplots centred on the median value. They look very similar and from Figure S6, it is difficult to see either improvement or degradation from the analysis.



For evapotranspiration, river discharge and surface soil moisture there is a slight advantage for  
525 LDAS\_ERA5 analysis with respect to its open-loop counterpart. Even if the distribution of the  
averaged statistical metrics can be rather similar for both (particularly true for surface soil moisture  
evaluation), there are significant regional differences for some sites, which shows the added value  
of the analysis with respect to the open-loop.

### 3.2 Monitoring and forecasts for areas under severe/extreme conditions

530 For each individual region presented in Table I and Figure 2, monthly anomalies (scaled by the  
standard deviation) of analysed SSM (second layer of soil, 1-4cm) and LAI for 2018 were assessed  
with respect to the 2010-2018 period. The anomalies (see Figure 8) highlight three regions, two  
presenting strong negative anomalies for both SSM and LAI for almost all 2018 (north western  
Europe, WEUR, and the Murray-Darling basin, MUDA, in south eastern Australia) and one  
535 presenting strong positive anomalies of SSM and LAI in Eastern Africa (EAFR). WEUR and  
MUDA regions were affected by a severe heatwave and a drought in 2018 impacting LSVs  
analysed by LDAS\_ERA5. According to Figure 8, monthly anomalies of SSM and LAI for MUDA  
are negative through the whole 2018 with 7 and 6 months presenting LAI and SSM anomalies  
below -1 standard deviation (stdev), respectively. WEUR has negative SSM anomalies from May to  
540 December 2018 with values going below -2 stdev. LAI was severely impacted as well with July to  
October 2018 presenting negative anomalies below -2 stdev. For WEUR, 5 months present LAI and  
SSM anomalies below -1 stdev. EAFR experiences 3 and 7 months with positive anomalies for  
SSM and LAI in 2018 above 1 stdev (8 and 7 months consecutively present positive anomalies for  
SSM and LAI respectively).

545 According to the National Oceanic and Atmospheric Administration (NOAA), Europe experienced  
its warmest summer since continental records began in 1910 at +2.16°C (Global Climate Report,  
<https://www.ncdc.noaa.gov/sotc/global/> last accessed April 2019). In Europe, temperature for the  
whole summer 2018 was above climatology. The summer 2018 heatwave in Europe is already  
reported in the scientific literature (e.g. Magnusson et al., 2018, Albergel et al., 2019, Blyverket et  
550 al., 2019). In its 70<sup>th</sup> Special Climate Statement, the Australian Bureau of Meteorology (BoM) has  
reported a very hot and dry summer 2018 in eastern Australia (BoM, 2019). Like much of Australia,  
the Murray Darling basin has experienced a remarkably dry and hot weather during 2018 . The  
annual maximum temperature for the Murray Darling basin as a whole was more than two degrees  
above average during 2018. The northern Murray–Darling Basin in particular was severely affected  
555 with inflows to all catchments persistently well below average (<http://www.bom.gov.au/state-of-the-climate/>, last visited: April 2019). Finally, the East Africa Seasonal Monitor based on the Famine

Early Warning System Network (FEWS) confirms above-average rainfall amounts as well as significantly greener than normal vegetation conditions (e.g., <https://reliefweb.int/report/somalia/east-africa-seasonal-monitor-july-27-2018>, last visited: April 2019). As this study focuses on monitoring and forecasting the impact of severe conditions on LSVs, WEUR and MUDA are selected for further investigation.

### 3.2.1 Case studies for assessing LDAS-Monde medium resolutions ( $0.25^\circ \times 0.25^\circ$ ) experiments

Figure 9 illustrates seasonal cycles of observed LAI (Figure 9a) and SWI (Figure 9e), LDAS\_ERA5 analysis and open-loop LAI (Figure 9b) and SWI (Figure 9f) for the WEUR domain. The last year (2018) is compared to an average of the previous years (2010-2017). From Figure 9a one may see the heatwave impact with a sharp drop in observed LAI values from June to November 2018 (solid green line). Such low LAI values have never been observed over the eight previous years (dashed green line for the 2010-2017 averaged along with the 2010-2017 minimum and maximum observations in shaded green). A similar behaviour is also visible in the ASCAT SWI dataset in Figure 9e with the lowest values ever reached in this 2010-2018 period. Over WEUR, LDAS\_ERA5 open-loop overestimates LAI in the second part of the year as already highlighted by several studies (e.g. Albergel et al., 2017, 2019). LDAS\_ERA5 analysis has a positive impact, reducing LAI values, as seen on Figure 9b (LAI open-loop in blue, analysis in red) and on Figure 9c representing RMSD seasonal cycles. LDAS\_ERA5 analysis also leads to an improvement in correlations for LAI (see Figure 9d). Similar conclusions can be drawn for SSM (Figure 9e to h). Note that for data assimilation and statistical scores, ASCAT SWI estimates were converted into the model space, in  $m^3m^{-3}$ , as detailed in section 2.3. Finally looking at the MUDA area (panels of Figure 10) similar positive impact from the analysis over the open-loop simulation is obtained. Almost all month of 2018 presents the lowest anomaly values for both SSM and LAI. For both MUDA and WEUR the smaller differences between LDAS\_ERA5 analysis and open-loop in 2018 than in 2010-2017 (Figure 9 b and f, Figure 10 b and f) also suggest that both extreme events were well captured in the atmospheric forcing used to drive LDAS\_ERA5 while the statistical scores presented in Figure 9 c, d, g, h as well as in Figure 10 c, d, g, h also suggest an improvement from the analysis over the open-loop simulation.

### 3.2.2 Case studies for assessing LDAS-Monde high resolutions ( $0.1^\circ \times 0.1^\circ$ ) experiments

For these two specific areas, LDAS-Monde was also run forced by HRES (LDAS\_HRES) at  $0.1^\circ \times 0.1^\circ$  spatial resolution over April 2016 to December 2018. Additionally to LDAS\_HRES analysis, forecast experiments with a lead time of 4-days and 8-days, initialised by either LDAS\_HRES

590 analysis or open-loop are presented for 2017-2018 (for SSM and LAI) in order to assess the impact of the initial conditions on the forecast of LSVs.

Upper panels of Figure 11 and Figure 12, illustrate seasonal RMSD (Figure 11a, 12a) and correlation (Figure 11b, 12b) values between SSM from the second layer of soil (1–4 cm) from LDAS-Monde forced by HRES (LDAS\_HRES, open-loop and analysis) and ASCAT SSM  
595 estimates over 2017-2018. Scores between SSM from the second layer of soil of LDAS\_HRES 4-day forecast (LDAS\_fc4, initialised by either the open-loop or analysis) and 8-day forecast (LDAS\_fc8, initialised by either the open-loop or analysis) and ASCAT SSM estimates are reported, also. From the upper panels of those figures one may notice a small improvement from the analysis (solid red line) over the open-loop simulation (solid blue line), slightly decreasing RMSD  
600 values and increasing correlations values. However no improvement (nor degradation) is visible from the 4-d and 8-d forecasts experiments initialised by LDAS\_HRES analysis over those initialised by LDAS\_HRES open-loop, they display very similar scores. LDAS\_HRES SSM is of better quality than LDAS\_fc4 and LDAS\_fc8. Note however that for the MUDA area, there is a small positive impact of the initialisation on the 4-d and 8-d forecast of surface soil moisture. Those  
605 results suggest that this fast evolving model variable (SSM between 1 cm and 4 cm depth) relies more on the atmospheric forcing than to initial conditions (at least within the forecast range presented in this study) and it can be assumed that the 4-day and 8-day atmospheric forecast from HRES is of lower quality than the first 24-h analysis. Results for LAI are different than for SSM (lower panels of Figure 11 and Figure 12). Firstly, there is a large improvement from the analysis (solid red line) over the open-loop (solid blue line), particularly in the LAI decaying phase (Boreal and Austral autumns mainly). Secondly, LDAS\_HRES open-loop (solid blue line), LDAS\_fc4 (dotted blue line) and LDAS\_fc8 (dashed blue line) initialised by LDAS\_HRES open-loop present very similar skills, so do LDAS\_fc4 and LDAS\_fc8 initialised by LDAS\_HRES analysis (dotted and dashed red lines, respectively). They outperform however skills of LDAS\_HRES  
615 open-loop, LDAS\_fc4 and LDAS\_fc8 initialised by LDAS\_HRES open-loop. This suggests that LAI relies more on its initial conditions than to the atmospheric forcing (at least within the forecast range presented in this study) and that forecasting LAI is also a matter of initial conditions. This is true for these two contrasted areas, WEUR and MUDA.

These results are corroborated by Figures 13 (for WEUR) and 14 (for MUDA), top rows illustrate  
620 SSM and bottom rows LAI. Figures 13(a) and 14(a) show RMSD values between LDAS\_HRES open-loop SSM (1-4 cm) and ASCAT SSM over 2017-2018 for the WEUR and MUDA domains, respectively. Due to the seasonal linear rescaling applied to ASCAT estimates, RMSD values are rather small. For the WEUR (MUDA) domain they range from 0 to 0.048 m<sup>3</sup>m<sup>-3</sup> (0 to 0.040 m<sup>3</sup>m<sup>-3</sup>).

Figures 13(b) and 14(b) represent maps of RMSD differences between LDAS\_HRES analysis (open-loop) and ASCAT SSM estimates over 2017-2018 for the WEUR and MUDA domains, as well. Both maps are dominated by negative values (in blue) indicating that RMSD values are smaller (better) when using LDAS\_HRES analysis than when using LDAS\_HRES open-loop. It is also worth-mentioning that no positive differences (i.e. a degradation from the analysis) are present in those maps. RMSD differences for the WEUR domain range from  $-0.004 \text{ m}^3\text{m}^{-3}$  to  $0.004 \text{ m}^3\text{m}^{-3}$  meaning that the analysis is improving them by about 8 %. For the MUDA domain, they are improved by about 15%. Figures 13(c), (d) 14(c),(d) are also maps of RMSD differences, they consider forecast experiments (LDAS\_fc4, LDAS\_fc8). It appears that for both domains, the impact from the initialisation is rather small with few coloured areas, strengthening previous results suggesting that to forecast SSM variable, forcing quality is more important than initial conditions. It is different for LAI, RMSD values for LDAS\_HRES open-loop are ranging between 0 and  $1.6 \text{ m}^2\text{m}^{-2}$  over WEUR, 0 and  $1 \text{ m}^2\text{m}^{-2}$  over MUDA (Figures 13(e) and 14(e)). RMSD values are improved by up to 37 % over WEUR and up to 60% over MUDA by the analysis (Figures 13(f) and 14(f)). Improvement from the analysis over the open-loop experiment is consistent through all the WEUR domain while it is mainly the south eastern part of the MUDA domain that is improved (the north western part has low RMSD values as the open-loop).

Similarly to Figures 13(a, b, c, d) panels of Figure 15 illustrates the impact of the analysis on SSM using correlations. This time, ASCAT SWI (i.e. no rescaling) has been used. Figure 15 (top panels) shows map of R values based on absolute values while Figure 15 (bottom panels) shows R values on anomalies (short term variability) as defined in Albergel et al., 2018a. Figure 15 (a) and (e) represents R values and anomaly R values for LDAS\_HRES, respectively. As expected R values are higher than anomaly R values. Maps of differences (panels b and f) of Figure 15 suggest that after assimilation, both scores are improved rather equally. While the 4 day and 8-day forecast still show an improvement from the initial condition on R values (panels c and d of Figure 15 dominated by positive differences, analysis minus open-loop), maps of anomaly R values forecast do not display any negative or positive impact (panels g and h of Figure 15).

Top panels of Figure 16 illustrate the impact of the analysis on drainage monitoring and forecast over WEUR. Fig. 16 a) represents drainage from LDAS\_HRES open-loop varying between 0 and  $1 \text{ kg.m}^{-2}.\text{day}^{-1}$ , as seen in Fig.16 b) (drainage difference between LDAS\_HRES analysis and openloop) analysis impact is rather small, about  $\pm 3\%$  and more pronounced in areas where the analysis has affected LAI more (see panels f), g) and h) of Figure 13). As seen on panels c) and d), there is also an impact from the initialisation in areas were the analysis was more effectively correcting LAI. Bottom panels of Figure 16 illustrate similar impact on runoff. As for drainage, this

variable is affected by the analysis. Initial conditions have an impact on its forecast, also. Although we did not present a quality assessment of those two variables, our findings on river discharge analysis impact, but also those from Albergel et al., 2017, 2018a, suggest a neutral to positive impact, propagated from the analysis of SSM and LAI to river discharge through variables such as drainage and runoff.

#### 4 Discussion and conclusion

This study has demonstrated that combining a LSM, satellite EOs and atmospheric forcing through LDAS-Monde has a great potential to represent the impact of extreme weather (heatwaves and droughts) on land surface conditions. LDAS-Monde is now ready for use in various applications such as (i) reanalyses of land Essential Climate Variables (ECVs), (ii) monitoring of water resources, drought and vegetation, and (iii) detection of severe conditions over land and initialisation of LSVs forecast. It has been applied in this study to past events of 2018 with respect to a short period of time (2010-2018) as a demonstrator but will be extended to longer time period. LDAS-Monde operational use in near real time has the capacity to serve as an emergency monitoring system for the LSVs. Using atmospheric reanalysis like ERA5 to force LDAS-Monde guarantees a high level of consistency because of its frozen configuration (no changes in spatial and vertical resolutions, data assimilation and parametrizations). The ERA5 coarse spatial resolution makes it affordable to run long term and large scale LDAS-Monde experiments. With ERA5 available from 1979 and now covering near real-time needs with its ERA5T version (<https://climate.copernicus.eu/climate-reanalysis>), an LDAS\_ERA5 configuration would be able to provide a long term and near real time coarse resolution ( $0.25^\circ \times 0.25^\circ$ ) climatology as reference for anomalies of the land surface conditions. Significant anomalies could then be used to trigger more focused “on-demand” simulations for regions experiencing extreme conditions. In that case LDAS-Monde could be run forced by e.g. ECMWF operational high resolution product ( $0.10^\circ \times 0.10^\circ$ ) in monitoring and forecast (up to 10-d ahead) modes, as was presented here for two regions in North Western Europe and South Eastern Australia. In term of RMSD, our results showed a very small impact of initial conditions on the forecasts of SSM. This was expected due to the reduced memory of the top soil surface (1-4 cm), which is dominated by meteorological variability. However, the LAI initialisation had significant impact on the LAI forecast skill. This was also expected due to the memory of vegetation evolution. For SSM, the assimilation is done after a rescaling to the model climatology (see section 2.3), which removes bias. For LAI, however this is not the case and the assimilation process removes bias in the modelled LAI (w.r.t. the observation). This technical difference between SSM and LAI assimilation, combined with the longer memory of LAI compared

to SSM, contributes to the results presented in this section. Despite the expected behaviour of these two LSVs in forecasting, our results show that LDAS-Monde system is capable of propagating the initial LAI conditions, which is relevant not only for LSV medium-range forecasting but with potential for longer lead-times. The strong impact of LAI initialisation on the forecast does not  
695 seem to propagate to surface soil moisture and further studies are necessary to test the impact of initial conditions to more variables from LDAS-Monde (including soil moisture in deeper layers and evapotranspiration). Another possibility would be to force LDAS-Monde using ECMWF ensemble forecasts, although the ensemble system has coarser spatial-resolution ( $\sim 0.20^\circ \times 0.20^\circ$ ), it offers a 15-day forecast and a 51 member ensemble, which can introduce forcing uncertainty into  
700 the LSVs. The maximum range of the soil and vegetation forecast could even reach up to six months if using seasonal atmospheric forecasts as forcing.

LDAS-Monde has well identified areas of developments that can further improve the representation of LSVs. For instance, it does not consider snow data assimilation yet and it has been shown in this study that the snow accumulation seems to be represented correctly in the system, it suffers from a  
705 too early snow-melt in spring. To overcome this issue, two possibilities will be explored. Firstly using a recently developed ISBA parametrisation, MEB for Multiple Energy Budget which is known to lead to a better representation of the snowpack (Boone et al., 2017), in particular in the densely forested areas of the Northern Hemisphere where large differences between LDAS-Monde and the IMS snow cover were found in spring (Figure S2(i), Aaron Boone CNRM, personal  
710 communication June 2019) and (ii) adapting the current data assimilation scheme of LDAS-Monde to permit assimilation the IMS snow cover data (as done e.g. at ECMWF, de Rosnay et al., 2014). The current SEKF data assimilation scheme is also being revisited. Even though it has provided good results, one of its limitations is the computation of a Jacobian matrix which requires one model run for each control variable, requiring significant computational resources with increased  
715 number of control variables. That is why more flexible Ensemble based approaches like the Ensemble Square Root Filter (EnSRF) have recently been implemented (Fairbain et al., 2015, Bonan et al., 2020). Bonan et al., 2020 have evaluated performances from the EnSRF and the SEKF over the Euro-Mediterranean area. Both data assimilation schemes have a similar behaviour for LAI while for SSM, EnSRF estimates tend to be closer to observations than those from the SEKF. They  
720 have also conducted an independent evaluation of both assimilation approaches using satellite estimates of evapotranspiration and GPP as well as measures of river discharges from gauging stations. They have found that the EnSRF leads to a systematic (moderate) improvement for evapotranspiration and GPP and a highly positive impact on river discharges, while the SEKF lead

to more contrasting performance. As for applications in hydrology, the 0.5° x 0.5° spatial resolution  
725 TRIP river network is currently being improved to 1/12° x 1/12° globally.

CNRM is also investigating the direct assimilation of ASCAT radar backscatter (Shamambo et al.,  
2019), it is supposed to tackle the way vegetation is accounted for in the change detection approach  
used to retrieve SSM with an improved representation of its effect. Assimilating ASCAT radar  
backscatter also raises the question of how to specify observation, background, and model error  
730 covariance matrices, so far mainly relying on soil properties (see section 2.1.3 on data assimilation).  
The last decade has seen the development of techniques to estimate those matrices. Approaches  
based on Desroziers diagnostics (Desroziers et al., 2005) are affordable for land data assimilation  
systems from a computational point of view and could provide insightful information on the various  
sources of the data assimilation system.

735 Also, the added value of LDAS-Monde compared to already existing datasets has to be evaluated  
and current work at Météo-France is investigating its quality against state of the art reanalyses such  
as those from NASA at either global scale (GLDAS, Rodell et al., 2004, MERRA-2, The Modern-  
Era Retrospective Analysis for Research and Applications, Version 2, Reichle et al., 2017, Draper et  
al., 2018) or regional scale (NCALDAS over the continental USA, FLDAS over Africa). Finally,  
740 first attempts to go to higher spatial resolution over smaller areas like the AROME domain  
(Applications de la Recherche à l'Opérationnel à Méso-Echelle, [https://www.umr-cnrm.fr/spip.php?  
article120](https://www.umr-cnrm.fr/spip.php?article120), last accessed July 2019) of Météo-France (centred over France) at kilometre scale and  
assimilating kilometric and sub-kilometric scale satellite retrieval of SSM and LAI (from CGLS)  
are very promising.

745

**Code availability.** LDAS-Monde is a part of the ISBA land surface model and is available as open  
source via the surface modelling platform called SURFEX. SURFEX can be downloaded freely at  
<http://www.umr-cnrm.fr/surfex/> using a CECILL-C Licence (a French equivalent to the L-GPL  
750 licence; [http://www.cecill.info/licences/Licence\\_CeCILL-C\\_V1-en.txt](http://www.cecill.info/licences/Licence_CeCILL-C_V1-en.txt)). It is updated at a relatively  
low frequency (every 3 to 6 months). If more frequent updates are needed, or if what is required is  
not in Open-SURFEX (DrHOOK, FA/LFI formats, GAUSSIAN grid), you are invited to follow the  
procedure to get a SVN account and to access real-time modifications of the code (see the  
instructions at the first link). The developments presented in this study stemmed on SURFEX  
755 version 8.1. LDAS-Monde technical documentation and contact point are freely available at: [https://  
opensource.umr-cnrm.fr/projects/openldasmonde/files](https://opensource.umr-cnrm.fr/projects/openldasmonde/files)

**Data availability:** upon request by contacting the corresponding author.

**Author Contributions:** Conceptualization, CA, JCC.; Investigation, CA, YZ, SM, NRF;  
760 Methodology, CA; Writing—original draft, CA; Writing—review and editing, All

**Funding:** This research was funded by IRT Antoine de Saint-Exupéry Foundation, grant number CDT-R056-L00-T00 (POMME-V project), the Climate Change Initiative Programme Extension, Phase 1 - Climate Modeling User Group ESA/contract No [4000125156/18/I-NB](#)

765 **Acknowledgments:** Results were generated using the Copernicus Climate Change Service Information, 2017. The Authors would like to thanks the Copernicus Global Land Service for providing the satellite derived Leaf Area Index and Surface Soil Moisture.

**Conflicts of Interest: The authors declare no conflict of interest**

770



## References

- Albergel, C.; Rüdiger, C.; Pellarin, T.; Calvet, J.-C.; Fritz, N.; Froissard, F.; Suquia, D.; Petitpa, A.; Pignatelli, B.; Martin, E. From near-surface to root-zone soil moisture using an exponential filter: An assessment of the method based on in-situ observations and model simulations. *Hydrol. Earth Syst. Sci.*, 12, 1323–1337, 2008.
- Albergel, C., Munier, S., Leroux, D. J., Dewaele, H., Fairbairn, D., Barbu, A. L., Gelati, E., Dorigo, W., Faroux, S., Meurey, C., Le Moigne, P., Decharme, B., Mahfouf, J.-F., and Calvet, J.-C.: Sequential assimilation of satellite-derived vegetation and soil moisture products using SURFEX\_v8.0: LDAS-Monde assessment over the Euro-Mediterranean area, *Geosci. Model Dev.*, 10, 3889–3912, <https://doi.org/10.5194/gmd-10-3889-2017>, 2017.
- Albergel, C.; Munier, S.; Bocher, A.; Bonan, B.; Zheng, Y.; Draper, C.; Leroux, D.J.; Calvet, J.-C. LDAS-Monde Sequential Assimilation of Satellite Derived Observations Applied to the Contiguous US: An ERA5 Driven Reanalysis of the Land Surface Variables. *Remote Sens.*, 10, 1627, 2018a
- Albergel, C.; Dutra, E.; Munier, S.; Calvet, J.-C.; Munoz-Sabater, J.; de Rosnay, P.; Balsamo, G. ERA-5 and ERA-Interim driven ISBA land surface model simulations: Which one performs better? *Hydrol. Earth Syst. Sci.*, 22, 3515–3532, 2018b.
- Albergel, C.; Dutra, E.; Bonan, B.; Zheng, Y.; Munier, S.; Balsamo, G.; de Rosnay, P.; Muñoz-Sabater, J.; Calvet, J.-C. Monitoring and Forecasting the Impact of the 2018 Summer Heatwave on Vegetation. *Remote Sens.*, 11, 520, 2019.
- Balsamo, G., Albergel, C., Beljaars, A., Boussetta, S., Brun, E., Cloke, H., Dee, D., Dutra, E., Muñoz-Sabater, J., Pappenberger, F., de Rosnay, P., Stockdale, T., and Vitart, F.: ERA-Interim/Land: a global land surface reanalysis data set, *Hydrol. Earth Syst. Sci.*, 19, 389–407, <https://doi.org/10.5194/hess-19-389-2015>, 2015.
- Balsamo, G.; Agustí-Panareda, A.; Albergel, C.; Arduini, G.; Beljaars, A.; Bidlot, J.; Bousserez, N.; Boussetta, S.; Brown, A.; Buizza, R.; Buontempo, C.; Chevallier, F.; Choulga, M.; Cloke, H.; Cronin, M.F.; Dahoui, M.; De Rosnay, P.; Dirmeyer, P.A.; Dutra, M.D.E.; Ek, M.B.; Gentile, P.; Hewitt, H.; Keeley, S.P.E.; Kerr, Y.; Kumar, S.; Lupu, C.; Mahfouf, J.-F.; McNorton, J.; Mecklenburg, S.; Mogensen, K.; Muñoz-Sabater, J.; Orth, R.; Rabier, F.; Reichle, R.; Ruston, B.; Pappenberger, F.; Sandu, I.; Seneviratne, S.I.; Tietsche, S.; Trigo, I.F.; Uijlenhoet, R.; Wedi, N.; Woolway, R.I.; Zeng, X. Satellite and In Situ Observations for Advancing Global Earth Surface Modelling: A Review. *Remote Sens.*, 10(12), 2038; <https://doi.org/10.3390/rs10122038>, 2018.
- Bamzai, A.; Shukla, J. Relation between Eurasian snow cover, snow depth and the Indian summer monsoon: An observational study. *J. Clim.*, 12, 3117–3132, 1999.
- Barbu, A.L.; Calvet, J.-C.; Mahfouf, J.-F.; Albergel, C.; Lafont, S. Assimilation of Soil Wetness Index and Leaf Area Index into the ISBA-A-gs land surface model: Grassland case study. *Biogeosciences*, 8, 1971–1986., 2011.
- Barbu, A. L., Calvet, J.-C., Mahfouf, J.-F., and Lafont, S.: Integrating ASCAT surface soil moisture and GEOV1 leaf area index into the SURFEX modelling platform: a land data assimilation application over France, *Hydrol. Earth Syst. Sci.*, 18, 173–192, <https://doi.org/10.5194/hess-18-173-2014>, 2014.
- Barella-Ortiz, A. and Quintana-Seguí, P.: Evaluation of drought representation and propagation in Regional Climate Model simulations over Spain, *Hydrol. Earth Syst. Sci. Discuss.*, <https://doi.org/10.5194/hess-2018-603>, in review, 2018.

- 815 Baret, F.; Weiss, M.; Lacaze, R.; Camacho, F.; Makhmarad, H.; Pacholczyk, P.; Smetse, B. GEOV1: LAI, FAPAR essential climate variables and FCOVER global time series capitalizing over existing products, Part 1: Principles of development and production. *Remote Sens. Environ.*, 137, 299–309, doi:10.1016/j.rse.2012.12.027, 2013.
- Bartalis, Z.; Wagner, W.; Naeimi, V.; Hasenauer, S.; Scipal, K.; Bonekamp, H.; Figa, J.; Anderson, C.: Initial soil moisture retrievals from the METOP-A advanced Scatterometer (ASCAT). *Geophys. Res. Lett.*, 34, L20401, doi: 10.1029/2007GL031088., 2007.
- Bauer, P.; Thorpe, A.; Brunet, G. The quiet revolution of numerical weather prediction. *Nature*, 525, 47–55, doi:10.1038/nature14956, 2015.
- Beck, H. E., Pan, M., Roy, T., Weedon, G. P., Pappenberger, F., van Dijk, A. I. J. M., Huffman, G. J., Adler, R. F., and Wood, E. F.: Daily evaluation of 26 precipitation datasets using Stage-IV gauge-radar data for the CONUS, *Hydrol. Earth Syst. Sci.*, 23, 207–224, <https://doi.org/10.5194/hess-23-207-2019>, 2019.
- 825 Bell, J. E., M. A. Palecki, C. B. Baker, W. G. Collins, J. H. Lawrimore, R. D. Leeper, M. E. Hall, J. Kochendorfer, T. P. Meyers, T. Wilson, and H. J. Diamond.: U.S. Climate Reference Network soil moisture and temperature observations. *J. Hydrometeorol.*, 14, 977–988. doi: 10.1175/JHM-D-12-0146.1, 2013.
- Bierkens, M.; van Beek, L. Seasonal predictability of European discharge: Nao and hydrological response time. *J. Hydrometeorol*, 10, 953–968, 2009.
- Blyverket, J.; Hamer, P.D.; Schneider, P.; Albergel, C.; Lahoz, W.A. Monitoring Soil Moisture Drought over Northern High Latitudes from Space. *Remote Sens.*, 11, 1200, 2019.
- 835 Bonan, B., Albergel, C., Zheng, Y., Barbu, A. L., Fairbairn, D., Munier, S., and Calvet, J.-C.: An ensemble square root filter for the joint assimilation of surface soil moisture and leaf area index within the Land Data Assimilation System LDAS-Monde: application over the Euro-Mediterranean region, *Hydrol. Earth Syst. Sci.*, 24, 325–347, <https://doi.org/10.5194/hess-24-325-2020>, 2020.
- 840 Boone, A.; Masson, V.; Meyers, T.; Noilhan, J. The influence of the inclusion of soil freezing on simulations by a soil-vegetation-atmosphere transfer scheme. *J. Appl. Meteorol.*, 39, 1544–1569, 2000.
- Boone, A. and Etchevers, P.: An intercomparison of three snow schemes of varying complexity coupled to the same land-surface model: local scale evaluation at an Alpine site, *J. Hydrometeorol.*, 2, 374–394, 2001.
- 845 Boone, A., Samuelsson, P., Gollvik, S., Napoly, A., Jarlan, L., Brun, E., and Decharme, B.: The interactions between soil–biosphere–atmosphere land surface model with a multi-energy balance (ISBA-MEB) option in SURFEXv8 – Part 1: Model description, *Geosci. Model Dev.*, 10, 843–872, <https://doi.org/10.5194/gmd-10-843-2017>, 2017.
- 850 Bruce, J.P., Natural disaster reduction and global change. *Bulletin of the American Meteorological Society*, 75(10): 1831–1835, 1994.
- Bureau of Meteorology Special Climate Statement 70: Drought conditions in eastern Australia and impact on water resources in the Murray–Darling Basin, Issued 9 April 2019, <http://www.bom.gov.au/climate/current/statements/scs70.pdf>, 2019.
- 855 Calvet, J.-C.; Noilhan, J.; Roujean, J.-L.; Bessemoulin, P.; Cabelguenne, M.; Olioso, A.; Wigneron, J.-P. An interactive vegetation SVAT model tested against data from six 780 contrasting sites. *Agric. For. Meteorol*, 92, 73–95, 1998.
- Calvet, J.-C.; Rivalland, V.; Picon-Cochard, C.; Guehl, J.-M. Modelling forest transpiration and CO<sub>2</sub> fluxes—Response to soil moisture stress. *Agric. For. Meteorol*, 124, 143–156, 2004.

- 860 Cook, E.R., Seager, R., Cane, M.A. and Stahle, D.W., North American drought: reconstructions, causes, and consequences. *Earth Science Reviews*, 81(1): 93–134, 2007.
- de Jeu, R.A.; Wagner, W.; Holmes, T.R.H.; Dolman, A.J.; Van De Giesen, N.C.; Friesen, J. Global soil moisture patterns observed by space borne microwave radiometers and scatterometers. *Surv. Geophys.*, 29, 399–420, 2008.
- 865 de Rosnay, P. A simplified Extended Kalman Filter for the global operational soil moisture analysis at ECMWF. *Q. J. R. Meteorol. Soc.*, 139, 1199–1213, doi: [10.1002/qj.2023](https://doi.org/10.1002/qj.2023), 2013.
- de Rosnay, P.; Balsamo, G.; Albergel, C.; Muñoz-Sabater, J.; Isaksen, L. Initialisation of land surface variables for numerical weather prediction. *Surv. Geophys.*, 35, 607–621, doi: [10.1007/s10712-012-9207-x](https://doi.org/10.1007/s10712-012-9207-x), 2014.
- 870 Desroziers, G.; Berre, L.; Chapnik, B.; Poli, P. Diagnosis of observation, background and analysis-error statistics in observation space. *Q. J. Roy. Meteor. Soc.*, 131, 3385–3396, 2005.
- Di Napoli, C., F. Pappenberger, and H.L. Cloke: Verification of Heat Stress Thresholds for a Health-Based Heat-Wave Definition. *J. Appl. Meteor. Climatol.*, 58, 1177–1194, <https://doi.org/10.1175/JAMC-D-18-0246.1>, 2019.
- 875 Decharme, B., Boone, A., Delire, C., and Noilhan, J.: Local evaluation of the Interaction between soil biosphere atmosphere soil multilayer diffusion scheme using four pedotransfer functions, *J. Geophys. Res.*, 116, D20126, <https://doi.org/10.1029/2011JD016002>, 2011.
- Decharme, B.; Martin, E.; Faroux, S. Reconciling soil thermal and hydrological lower boundary conditions in land surface models. *J. Geophys. Res. Atmos.*, 118, 7819–7834, 2013.
- 880 Decharme, B., Brun, E., Boone, A., Delire, C., Le Moigne, P., and Morin, S.: Impacts of snow and organic soils parameterization on northern Eurasian soil temperature profiles simulated by the ISBA land surface model, *The Cryosphere*, 10, 853–877, <https://doi.org/10.5194/tc-10-853-2016>, 2016.
- Decharme, B., Delire, C., Minvielle, M., Colin, J., Vergnes, J.-P., Alias, A., Saint-Martin, D., Séférian, R., Sénési, S. and Voldoire, A.: Recent changes in the ISBA-CTRIP Land Surface System for use in the CNRM-CM6 climate model and in global off-line hydrological applications, *J. Adv. Model Earth Sy.*, 11, 1207-1252, [10.1029/2018MS001545](https://doi.org/10.1029/2018MS001545), 2019.
- 885 Dee, D.P.; Uppala, S.M.; Simmons, A.J.; Berrisford, P.; Poli, P.; Kobayashi, S.; Andrae, U.; Balmaseda, M.A.; Balsamo, G.; Bauer, D.P. The ERA-Interim reanalysis: Configuration and performance of the data assimilation system. *Q. J. R. Meteorol. Soc.*, 137, 553–597, 2011.
- 890 Dirmeyer, P. A., Gao, X., Zhao, M., Guo, Z., Oki, T., and Hanasaki N.: The Second Global Soil Wetness Project (GSWP-2): Multi-model analysis and implications for our perception of the land surface, *B. Am. Meteorol. Soc.*, 87, 1381–1397, <https://doi.org/10.1175/BAMS-87-10-1381>, 2006.
- Dorigo, W. A., Wagner, W., Hohensinn, R., Hahn, S., Paulik, C., Xaver, A., Gruber, A., Drusch, M., Mecklenburg, S., van Oevelen, P., Robock, A., and Jackson, T.: The International Soil Moisture Network: a data hosting facility for global in situ soil moisture measurements, *Hydrol. Earth Syst. Sci.*, 15, 1675-1698, <https://doi.org/10.5194/hess-15-1675-2011>, 2011.
- 895 Dorigo, W.A., A. Gruber, R.A.M. De Jeu, W. Wagner, T. Stacke, A. Loew, C. Albergel, L. Brocca, D. Chung, R.M. Parinussa and R. Kidd: Evaluation of the ESA CCI soil moisture product using ground-based observations, *Remote Sensing of Environment*, <http://dx.doi.org/10.1016/j.rse.2014.07.023>, 2015.
- 900 Draper, C. S., Mahfouf, J.-F., and Walker, J. P.: An EKF assimilation of AMSR-E soil moisture into the ISBA land surface scheme, *J. Geophys. Res.*, 114, D20104, <https://doi.org/10.1029/2008JD011650>, 2009.

- 905 Draper, C.; Mahfouf, J.-F.; Calvet, J.-C.; Martin, E.; Wagner, W. Assimilation of ASCAT near-surface soil moisture into the SIM hydrological model over France. *Hydrol. Earth Syst. Sci.*, 15, 3829–3841, 2011.
- Draper, C. S., R. H. Reichle, and R. D. Koster, Assessment of MERRA-2 Land Surface Energy Flux Estimates, *Journal of Climate*, 31, 671–691, doi:10.1175/JCLI-D-17-0121.1, 2018.
- 910 Faroux, S.; Kaptué Tchuenté, A.T.; Roujean, J.-L.; Masson, V.; Martin, E.; Moigne, P.L. ECOCLIMAP-II/Europe: A twofold database of ecosystems and surface parameters at 1 km resolution based on satellite information for use in land surface, meteorological and climate models. *Geosci. Model Dev.*, 6, 563–582, 2013.
- Fairbairn, D., Barbu, A. L., Mahfouf, J.-F., Calvet, J.-C. and Gelati, E.: Comparing the ensemble and extended Kalman filters for in situ soil moisture assimilation with contrasting conditions, *Hydrol. Earth Syst. Sci.*, 19, 4811–4830, doi: [10.5194/hess-19-4811-2015](https://doi.org/10.5194/hess-19-4811-2015), 2015.
- 915 Fairbairn, D.; Barbu, A.L.; Napoly, A.; Albergel, C.; Mahfouf, J.-F.; Calvet, J.-C. The effect of satellite-derived surface soil moisture and leaf area index land data assimilation on streamflow simulations over France. *Hydrol. Earth Syst. Sci.*, 21, 2015–2033, 2017.
- Fox, A.M.; Hoar, T.J.; Anderson, J.L.; Arellano, A.F.; Smith, W.K.; Litvak, M.E.; MacBean, N.; 920 Schimel, D.S.; Moore, D.J.P. Evaluation of a Data Assimilation System for Land Surface Models using CLM4.5. *J. Adv. Model. Earth Syst.*, 10, 2471–24942, 2018.
- Gibelin, A.-L.; Calvet, J.-C.; Roujean, J.-L.; Jarlan, L.; Los, S.O. Ability of the land surface model ISBA-A-gs to simulate leaf area index at global scale: Comparison with satellite products. *J. Geophys. Res.*, 111, 1–16, 2006.
- 925 Gruber, A.; Su, C.-H.; Zwieback, S.; Crow, W.; Dorigo, W.; Wagner, W. Recent advances in (soil moisture) triple collocation analysis. *Int. J. Appl. Earth Obs. Geoinf.*, 45, 200–211, 2016.
- Hersbach, H., de Rosnay, P. Bell, B., Schepers, D., Simmons, S., Soci, S., Abdalla, S., Alonso Balmaseda, M., Balsamo, G., Bechtold, P., Berrisford, P., Bidlot, J., de Boissésón, E., Bonavita, M., Browne, P., Buizza, R., Dahlgren, P., Dee, D., Dragani, R., Diamantakis, M., Flemming, J., Forbes, 930 R., Geer, A., Haiden, T., Hólm, E., Haimberger, L., Hogan, R., Horányi, A., Janisková, M., Laloyaux, P., Lopez, P., Muñoz-Sabater, J., Peubey, C., Radu, R., Richardson, D., Thépaut, J.-N., Vitart, F., Yang, X., Zsótér, E. and Zuo H. Operational global reanalysis: Progress, future directions and synergies with NWP. *ERA Rep. Ser.*, 27, 65., 2018.
- Hersbach, H., B. Bell, P. Berrisford, S. Hirahara, A. Horanyi, J. Muñoz-Sabater, J. Nicolas, C. 935 Peubey, R. Radu, D. Schepers, A. Simmons, C. Soci, S. Abdalla, X. Abellan, G. Balsamo, P. Bechtold, G. Biavati, J. Bidlot, M. Bonavita, G. De Chiara, P. Dahlgren, D. Dee, M. Diamantakis, R. Dragani, J. Flemming, R. Forbes, M. Fuentes, A. Geer, L. Haimberger, S. Healy, R. J. Hogan, E. Holm, M. Janiskova, S. Keeley, P. Laloyaux, P. Lopez, G. Radnoti, P. de Rosnay, I. Rozum, F. Vamborg, S. Villaume, J.-N. Thépaut: The ERA5 Global Reanalysis, *QJRMS*, submitted, 2019
- 940 IPCC: Managing the Risks of Extreme Events and Disasters to Advance Climate Change Adaptation. A Special Report of Working Groups I and II of the Intergovernmental Panel on Climate Change . Cambridge University Press, Cambridge, UK, and New York, NY, USA, 582 pp, 2012.
- 945 IPCC: Climate change 2014: Synthesis Report. Contribution of Working Groups I, II and III to the Fifth Assessment Report of the Intergovernmental Panel on Climate Change [Core Writing Team, R.K. Pachauri and L.A. Meyer (eds.)]. IPCC, Geneva, Switzerland, 151 pp, 2014.
- Jacobs, C.M.J.; van den Hurk, B.J.J.M.; de Bruin, H.A.R. Stomatal behaviour and photosynthetic rate of unstressed grapevines in semi-arid conditions. *Agric. For. Meteorol.* 80, 111–134, 1996.

- 950 Jarlan, L., Balsamo, G., Lafont, S., Beljaars, A., Calvet, J.-C., and Mougou, E.: Analysis of leaf area index in the ECMWF land surface model and impact on latent heat on carbon fluxes: Application to West Africa, *J. Geophys. Res.*, 113, D24117, doi:10.1029/2007JD009370, 2008.
- Joiner, J.; Yoshida, Y.; Guanter, L.; Middleton, E.M. New methods for the retrieval of chlorophyll red fluorescence from hyperspectral satellite instruments: Simulations and application to GOME-2 and SCIAMACHY. *Atmos. Meas. Tech.* 2016, 9, 3939–3967, 2016.
- 955 Jung, M., Reichstein, M., Schwalm, C. R., Huntingford, C., Sitch, S., Ahlström, A., Arneth, A., Camps-Valls, G., Ciais, P., Friedlingstein, P., Gans, F., Ichii, K., Jain, A. K., Kato, E., Papale, D., Poulter, B., Raduly, B., Rödenbeck, C., Tramontana, G., Viovy, N., Wang, Y.-P., Weber, U., Zaehle, S., and Zeng, N.: Compensatory water effects link yearly global land CO<sub>2</sub> sink changes to temperature, *Nature*, 541, 516–520, <https://doi.org/10.1038/nature20780>, 2017.
- 960 Ionita, M., Tallaksen, L. M., Kingston, D. G., Stagge, J. H., Laaha, G., Van Lanen, H. A. J., Scholz, P., Chelcea, S. M., and Haslinger, K.: The European 2015 drought from a climatological perspective, *Hydrol. Earth Syst. Sci.*, 21, 1397-1419, <https://doi.org/10.5194/hess-21-1397-2017>, 2017.
- 965 Kaminski, T. Assimilating atmospheric data into a terrestrial biosphere model: A case study of the seasonal cycle. *Glob. Biogeochem. Cycles*, 16, 2002.
- Kidd, R.; Makhmara, H.; Paulik, C. GIO GL1 PUM SWI I1.00.pdf., p. 25. Available online: <http://land.copernicus.eu/global/products/SWI/Documents/ProductUserManual> (accessed on 1 June 2019), 2013.
- 970 Kumar, S.V., B.F. Zaitchik, C.D. Peters-Lidard, M. Rodell, R. Reichle, B. Li, M. Jasinski, D. Mocko, A. Getirana, G. De Lannoy, M.H. Cosh, C.R. Hain, M. Anderson, K.R. Arsenault, Y. Xia, and M. Ek: [Assimilation of Gridded GRACE Terrestrial Water Storage Estimates in the North American Land Data Assimilation System](#). *J. Hydrometeorol.*, 17, 1951–1972, <https://doi.org/10.1175/JHM-D-15-0157.1>, 2016
- 975 Kumar, S.V.; Jasinski, M.; Mocko, D.; Rodell, M.; Borak, J.; Li, B.; Kato Beaudoin, H.; Peters-Lidard, C.D. NCA-LDAS land analysis: Development and performance of a multisensor, multi-variate land data assimilation system for the National Climate Assessment. *J. Hydrometeorol.*, doi:10.1175/JHM-D-17-0125.1., 2018.
- 980 Kumar, S.V., D.M. Mocko, S. Wang, C.D. Peters-Lidard, and J. Borak, 0: Assimilation of remotely sensed Leaf Area Index into the Noah-MP land surface model: Impacts on water and carbon fluxes and states over the Continental U.S.. *J. Hydrometeorol.*, [https://doi.org/10.1175/JHM-D-18-0237.1.](https://doi.org/10.1175/JHM-D-18-0237.1), 2019.
- Koster, R.D.; Mahanama, S.P.P.; Livneh, B.; Lettenmaier, D.P.; Reichle, R.H. Skill in streamflow forecasts derived from large-scale estimates of soil moisture and snow. *Nat. Geosci. Lett.*, 3, 613–616, 2010.
- 985 Lahoz, W.; De Lannoy; G. Closing the gaps in our knowledge of the hydrological cycle over land: Conceptual problems. *Surv. Geophys.*, 35, 577–606, 2014.
- Leroux, D.J.; Calvet, J.-C.; Munier, S.; Albergel, C. Using Satellite-Derived Vegetation Products to Evaluate LDAS-Monde over the Euro-Mediterranean Area. *Remote Sens.*, 10, 1199, 2014.
- 990 Luo, L.; Wood, E.F. Monitoring and predicting the 2007 U.S. drought. *Geophysical Research Letters*, 34. doi:10.1029/2007GL031673, 2007.
- Magnusson, L.; Ferranti, L.; Vamborg, F. Forecasting the 2018 European heatwave. *ECMWF Newslett.*, 157, 4, 2018.

- 995 Mahfouf, J.-F.; Bergaoui, K.; Draper, C.; Bouyssel, F.; Taillefer, F.; Taseva, L. A comparison of two off-line soil analysis schemes for assimilation of screen level observations. *J. Geophys. Res.*, 114, D08105, 2009.
- Martens, B., Miralles, D. G., Lievens, H., van der Schalie, R., de Jeu, R. A. M., Fernández-Prieto, D., Beck, H. E., Dorigo, W. A., and Verhoest, N. E. C.: GLEAM v3: satellite-based land evaporation and root-zone soil moisture, *Geosci. Model Dev.*, 10, 1903–1925, <https://doi.org/10.5194/gmd-10-1903-2017>, 2017.
- 1000 Massari, C.; Camici, S.; Ciabatta, L.; Brocca, L. Exploiting Satellite-Based Surface Soil Moisture for Flood Forecasting in the Mediterranean Area: State Update Versus Rainfall Correction. *Remote Sens.*, 10, 292, 2018.
- 1005 Masson, V., Le Moigne, P., Martin, E., Faroux, S., Alias, A., Alkama, R., Belamari, S., Barbu, A., Boone, A., Bouyssel, F., Brousseau, P., Brun, E., Calvet, J.-C., Carrer, D., Decharme, B., Delire, C., Donier, S., Essaouini, K., Gibelin, A.-L., Giordani, H., Habets, F., Jidane, M., Kerdraon, G., Kourzeneva, E., Lafaysse, M., Lafont, S., Lebeaupin Brossier, C., Lemonsu, A., Mahfouf, J.-F., Marguinaud, P., Mokhtari, M., Morin, S., Pigeon, G., Salgado, R., Seity, Y., Taillefer, F., Tanguy, G., Tulet, P., Vincendon, B., Vionnet, V., and Voldoire, A.: The SURFEXv7.2 land and ocean surface platform for coupled or offline simulation of earth surface variables and fluxes, *Geosci. Model Dev.*, 6, 929–960, <https://doi.org/10.5194/gmd-6-929-2013>, 2013.
- 1010 McNally, A., Arsenault, K., Kumar, S., Shukla, S., Peterson, P., Wang, S., Funk, C., Peters-Lidard, C.P., Verdin, J.P. A land data assimilation system for sub-Saharan Africa food and water security applications. *Sci. Data* 4:170012 <https://doi.org/10.1038/sdata.2017.12>, 2017
- 1015 Mishra, A.K. and Singh, V.P., A review of drought concepts. *Journal of Hydrology*, 391(1): 202–216, 2010.
- Miralles, D.G., De Jeu, R.A.M., Gash, J.H., Holmes, T.R.H., Dolman, A.J., Magnitude and variability of land evaporation and its components at the global scale. *Hydrol. Earth Syst. Sci.* 15 (3), 967–981. <http://dx.doi.org/10.5194/hess-15-967-2011>, 2011.
- 1020 Nash, J. E. and Sutcliffe, V.: River forecasting through conceptual models, *J. Hydrol.*, 10, 282–290, 1970.
- Noilhan, J. and Planton, S.: A simple parameterization of land surface processes for meteorological models. *Mon. Weather Rev.*, 117, 536–549, doi: [10.1175/1520-0493\(1989\)117<0536%3AASPOLS>2.0.CO;3B2](https://doi.org/10.1175/1520-0493(1989)117<0536%3AASPOLS>2.0.CO;3B2), 1989.
- 1025 Noilhan, J.; Mahfouf, J.-F. The ISBA land surface parameterisation scheme. *Glob. Planet. Chang.*, 13, 145–159, 1996
- Muñoz-Sabater, J. , Lawrence, H. , Albergel, C. , de Rosnay, P. , Isaksen, L. , Mecklenburg, S. , Kerr, Y. and Drusch, M., Assimilation of SMOS brightness temperatures in the ECMWF Integrated Forecasting System. *Q J R Meteorol Soc.* Accepted Author Manuscript. doi:[10.1002/qj.3577](https://doi.org/10.1002/qj.3577), 2019.
- 1030 Munro, R.; Eisinger, M.; Anderson, C.; Callies, J.; Corpaccioli, E.; Lang, R.; Lefebvre, A.; Livschitz, Y.; Perez Albinana, A. GOME-2 on MetOp: From In-Orbit Verification to Routine Operations. In *Proceedings of the EUMETSAT Meteorological Satellite Conference*, Helsinki, Finland, 12–16 June 2006.
- Obasi, G.O.P., WMO’s role in the international decade for natural disaster reduction. *Bulletin of the American Meteorological Society*, 75(9): 1655–1661, 1994.
- 1035 Orsolini, Y., Wegmann, M., Dutra, E., Liu, B., Balsamo, G., Yang, K., de Rosnay, P., Zhu, C., Wang, W., and Senan, R.: Evaluation of snow depth and snow-cover over the Tibetan Plateau in global

- reanalyses using in-situ and satellite remote sensing observations, *The Cryosphere Discuss.*, <https://doi.org/10.5194/tc-2019-49>, in review, 2019.
- 1040 Reichle, R.H.; Koster, R.D.; Liu, P.; Mahanama, S.P.P.; Njoku, E.G.; Owe, M. Comparison and assimilation of global soil moisture retrievals from the Advanced Microwave Scanning Radiometer for the Earth Observing System (AMSR-E) and the Scanning Multichannel Microwave Radiometer (SMMR). *J. Geophys. Res.*, 112, D09108, doi:10.1029/2006JD008033, 2007.
- 1045 Reichle, R. H., C. S. Draper, Q. Liu, M. Girotto, S. P. P. Mahanama, R. D. Koster, and G. J. M. De Lannoy, Assessment of MERRA-2 land surface hydrology estimates, *Journal of Climate*, **30**, 2937-2960, doi:10.1175/JCLI-D-16-0720.1, 2017.
- Reichle, R. H., Liu, Q., Koster, R. D., Crow, W. T., De Lannoy, G. J. M., Kimball, J. S., Ardizzone, J.V., Bosch, D., Colliander, A., Cosh, M., Kolassa, J., Mahanama, S.P., Prueger, J., Starks, P., Walker, J.P., Version 4 of the SMAP Level-4 Soil Moisture Algorithm and Data Product. *Journal of Advances in Modeling Earth Systems*, 11. <https://doi.org/10.1029/2019MS001729>, 2019.
- 1050 Rodell, M.; Houser, P.R.; Jambor, U.; Gottschalck, J.; Mitchell, K.; Meng, C.-J.; Arsenault, K.; Cosgrove, B.; Radakovich, J.; Bosilovich, M.; Entin, J.K., Walker, J.P., Lohmann, D., and Toll, D. The Global Land Data Assimilation System. *Bull. Am. Meteor. Soc.* 85, 381–394, 2004.
- Rodríguez-Fernández, N.; de Rosnay, P.; Albergel, C.; Richaume, P.; Aires, F.; Prigent, C.; Kerr, Y. SMOS Neural Network Soil Moisture Data Assimilation in a Land Surface Model and Atmospheric Impact. *Remote Sens.*, 11, 1334. <https://doi.org/10.3390/rs11111334>, 2019.
- 1055 Rüdiger, C.; Albergel, C.; Mahfouf, J.-F.; Calvet, J.-C.; Walker, J.P. Evaluation of Jacobians for leaf area index data assimilation with an extended Kalman filter. *J. Geophys. Res.* 2010.
- Sawada, Y.; Koike, T. Simultaneous estimation of both hydrological and ecological parameters in an ecohydrological model by assimilating microwave signal. *J. Geophys. Res. Atmos*, 119, 2014.
- 1060 Sawada, Y.; Koike, T.; Walker, J.P. A land data assimilation system for simultaneous simulation of soil moisture and vegetation dynamics. *J. Geophys. Res. Atmos*, 120, 2015.
- Schellekens, J., Dutra, E., Martínez-de la Torre, A., Balsamo, G., van Dijk, A., Sperna Weiland, F., Minvielle, M., Calvet, J.-C., Decharme, B., Eisner, S., Fink, G., Flörke, M., Peßenteiner, S., van Beek, R., Polcher, J., Beck, H., Orth, R., Calton, B., Burke, S., Dorigo, W., and Weedon, G. P.: A global water resources ensemble of hydrological models: the earthH2Observe Tier-1 dataset, *Earth Syst. Sci. Data*, 9, 389-413, <https://doi.org/10.5194/essd-9-389-2017>, 2017.
- 1065 Scipal, K.; Drusch, M.; Wagner, W. Assimilation of a ERS scatterometer derived soil moisture index in the ECMWF numerical weather prediction system. *Adv. Water Resour.*, 31, 1101–1112, 2008.
- Schlosser, A.; Dirmeyer, P. Potential predictability of Eurasian snow cover. *Atmos. Sci. Lett.*, 2, 1–8, 2001.
- 1070 Shamambo, D.C.; Bonan, B.; Calvet, J.-C.; Albergel, C.; Hahn, S. Interpretation of ASCAT Radar Scatterometer Observations Over Land: A Case Study Over Southwestern France. *Remote Sens.*, 11, 2842, 2019.
- Svoboda, M. Drought Monitor. *Bulletin of the American Meteorological Society*, pp. 1181–1190. doi:10.1175/1520-0477(2002)083<1181:TDM>2.3.CO;2., 2002
- 1075 Tall, M.; Albergel, C.; Bonan, B.; Zheng, Y.; Guichard, F.; Dramé, M.S.; Gaye, A.T.; Sintondji, L.O.; Hountondji, F.C.C.; Nikiema, P.M.; Calvet, J.-C. Towards a Long-Term Reanalysis of Land Surface Variables over Western Africa: LDAS-Monde Applied over Burkina Faso from 2001 to 2018. *Remote Sens.*, 11, 735, 2019.

- 1080 Tramontana, G., Jung, M., Schwalm, C. R., Ichii, K., Camps-Valls, G., Ráduly, B., Reichstein, M., Arain, M. A., Cescatti, A., Kiely, G., Merbold, L., Serrano-Ortiz, P., Sickert, S., Wolf, S., and Papale, D.: Predicting carbon dioxide and energy fluxes across global FLUXNET sites with regression algorithms, *Biogeosciences*, 13, 4291–4313, <https://doi.org/10.5194/bg-13-4291-2016>, 2016.
- 1085 Urraca, R.; Huld, T.; Gracia-Amillo, A.; Martinez-de-Pison, F.J.; Kaspar, F.; Sanz-Garcia, A. Evaluation of global horizontal irradiance estimates from ERA5 and COSMO-REA6 reanalyses using ground and satellite-based data. *Sol. Energy*, 164, 339–354, 2018.
- Van Loon, A.F.: Hydrological drought explained. *WIREs Water*, 2:359–392, doi:10.1002/wat2.1085, 2015.
- 1090 Voltaire, A., Decharme, B., Pianezze, J., Lebeaupin Brossier, C., Sevault, F., Seyfried, L., Garnier, V., Bielli, S., Valcke, S., Alias, A., Accensi, M., Arduin, F., Bouin, M.-N., Ducrocq, V., Faroux, S., Giordani, H., Léger, F., Marsaleix, P., Rainaud, R., Redelsperger, J.-L., Richard, E., and Riette, S.: SURFEX v8.0 interface with OASIS3-MCT to couple atmosphere with hydrology, ocean, waves and sea-ice models, from coastal to global scales, *Geosci. Model Dev.*, 10, 4207–4227, <https://doi.org/10.5194/gmd-10-4207-2017>, 2017.
- 1095 Wagner, W.; Lemoine, G.; Rott, H. A method for estimating soil moisture from ERS scatterometer and soil data. *Remote Sens. Environ.*, 70, 191–207, 1999.
- Wilhite, D.A., Drought, a global assessment. *Natural Hazards and Disasters Series*, vol. 1. Routledge, London, UK, 2000.
- 1100 World Meteorological Organization (WMO) and Global Water Partnership (GWP). Benefits of action and costs of inaction: Drought mitigation and preparedness – a literature review (N. Gerber and A. Mirzabaev). Integrated Drought Management Programme (IDMP) Working Paper 1. WMO, Geneva, Switzerland and GWP, Stockholm, Sweden, 2017.
- Xia, Y., Mitchell, K., Ek, M., Sheffield, J., Cosgrove, B., Wood, E., Luo, L., Alonge, C., Wei, H., 1105 Meng, J., Livneh, B., Lettenmaier, D., Koren, V., Duan, Q., Mo, K., Fan, Y. and Mocko, D., Continental-scale water and energy flux analysis and validation for the North American Land Data Assimilation System project phase 2 (NLDAS-2): 1. Intercomparison and application of model products, *J. Geophys. Res.*, 117, D03109, doi:[10.1029/2011JD016048](https://doi.org/10.1029/2011JD016048), 2012.
- Xia, Y., Mitchell K., Ek M., Cosgrove B., Sheffield J., Luo L., Alonge C., Wei H., Meng J., Livneh 1110 B., Duan Q. and Lohmann D.; Continental-scale water and energy flux analysis and validation for North American Land Data Assimilation System project phase 2 (NLDAS-2): 2. Validation of model-simulated streamflow, *J. Geophys. Res.*, 117, D03110, doi:[10.1029/2011JD016051](https://doi.org/10.1029/2011JD016051), 2012.



## Tables

1115 Table I: Continental hot spots for droughts and heat waves and number of monthly anomalies SSM and LAI below -1 standard deviation (stdev), above 1 stdev in 2018 with respect to the 2010-2018 period.

Region name	abbreviation	LON-W	LON-E	LAT-S	LAT-N	Number of monthly SSM anomalies below -1 (above 1) stdev	Number of monthly LAI anomalies below -1 (above 1) stdev
<b>Western-Europe</b>	<b>WEUR</b>	<b>-1</b>	<b>15</b>	<b>48</b>	<b>55</b>	<b>5(1)</b>	<b>5(0)</b>
Western Mediterranean	WMED	-10	15	35	45	0(7)	4(4)
Eastern Europe	EEUR	15	30	45	55	2(1)	0(2)
Balkans	BALK	15	30	40	45	3(3)	1(4)
Western Russia	WRUS	30	60	55	67	0(1)	1(3)
Lower Volga	LVOL	30	60	45	55	2(1)	2(1)
India	INDI	73	85	12	27	3(0)	2(1)
Southwestern China	SWCH	100	110	20	32	0(2)	0(6)
Northern China	NRCH	110	120	30	40	0(3)	0(4)
<b>Murray-Darling</b>	<b>MUDA</b>	<b>140</b>	<b>150</b>	<b>-37</b>	<b>-26</b>	<b>6(0)</b>	<b>7(0)</b>
California	CALF	-125	-115	30	42	2(0)	5(0)
Southern Plains	SPLN	-110	-90	25	37	0(3)	0(4)
Midwest	MIDW	-105	-85	37	50	1(2)	1(3)
Eastern North	ENRT	-85	-70	37	50	0(3)	0(7)
Nordeste	NDST	-44	-36	-20	-2	0(3)	1(2)
Pampas	PAMP	-64	-58	-36	-23	2(2)	2(0)
Sahel	SAHL	-18	25	13	19	2(0)	1(2)
<b>East Africa</b>	<b>EAFR</b>	<b>38</b>	<b>51</b>	<b>-4</b>	<b>12</b>	<b>2(3)</b>	<b>1(7)</b>
Southern Africa	SAFR	14	26	-35	-26	2(0)	2(1)

1120

Table II: Set up of the experiment used in this study. LDAS\_ERA5 and LDAS\_HRES have an analysis (assimilation of surface soil moisture, SSM, and leaf area index, LAI) and a model equivalent (open-loop, no assimilation), LDAS\_fc4 and LDAS\_fc8 are model runs initialized by either LDAS\_HRES open-loop or analysis. N/A stands for not applicable.

<b>Experiments (time period)</b>	<b>Model version</b>	<b>Atmospheric forcing</b>	<b>Domain &amp; spatial resolution</b>	<b>DA method</b>	<b>Assimilated observations</b>	<b>Model equivalents</b>	<b>Control variables</b>
LDAS_ERA5 (2010 to 2018)	ISBA Multi-layer soil model CO <sub>2</sub> -responsive version (Interactive vegetation)	ERA5	Global, ~0.25 °x 0.25°	SEKF	SSM (ASCAT)	Second layer of soil (1-4cm)	Layers of soil 2 to 8 (1-100cm)
LDAS_HRES (04/2016 to 12/2018)		IFS-HRES	North Western Europe ( <b>WEUR</b> ) and Murray-Darling River basin ( <b>MUDA</b> ) (see spatial extend in Table I) ~0.10° x 0.10°		LAI (GEOV1)	LAI	LAI
LDAS_fc4 (2017 to 2018)				N/A	N/A	N/A	N/A
LDAS_fc8 (2017 to 2018)		N/A	N/A	N/A	N/A		

1125 Table III: Evaluation datasets and associated metrics used in this study.

<b>Datasets used for the evaluation</b>	<b>Source</b>	<b>Metrics associated</b>
In situ measurements of soil moisture (ISMN Dorigo et al., 2011, 2015)	<a href="https://ismn.geo.tuwien.ac.at/en/">https://ismn.geo.tuwien.ac.at/en/</a>	R for both absolute and anomaly time-series, unbiased RMSD and bias
In situ measurements of river discharge	See Table S1	Nash Efficiency (NSE), Normalized Information Contribution (NIC) based on NSE,
In situ measurements of evapotranspiration (FLUXNET-2015)	<a href="http://fluxnet.fluxdata.org/data/fluxnet2015-dataset/">http://fluxnet.fluxdata.org/data/fluxnet2015-dataset/</a>	R, unbiased RMSD, Bias, NIC on R values
Satellite derived surface soil wetness index (ASCAT, Wagner et al., 1999, Bartalis et al., 2007)	<a href="http://land.copernicus.eu/global/">http://land.copernicus.eu/global/</a>	R and RMSD
Satellite derived Leaf Area Index (GEOV1, Baret et al., 2013)	<a href="http://land.copernicus.eu/global/">http://land.copernicus.eu/global/</a>	R and RMSD
Satellite-driven model estimates of land evapotranspiration (GLEAM, Martens et al., 2017)	<a href="http://www.gleam.eu">http://www.gleam.eu</a>	R and RMSD
Upscaled estimates of Gross Primary Production (GPP, Jung et al., 2017)	<a href="https://www.bgc-jenna.mpg.de/geodb/projects/Home.php">https://www.bgc-jenna.mpg.de/geodb/projects/Home.php</a>	R and RMSD
Solar Induced Fluorescence (SIF) from GOME-2 (Munro et al., 2006, Joiner et al., 2016)	See references	R
Interactive Multi-sensor Snow and Ice Mapping System (or IMS) snow cover	<a href="https://www.natice.noaa.gov/ims/">https://www.natice.noaa.gov/ims/</a>	Differences

## Figures

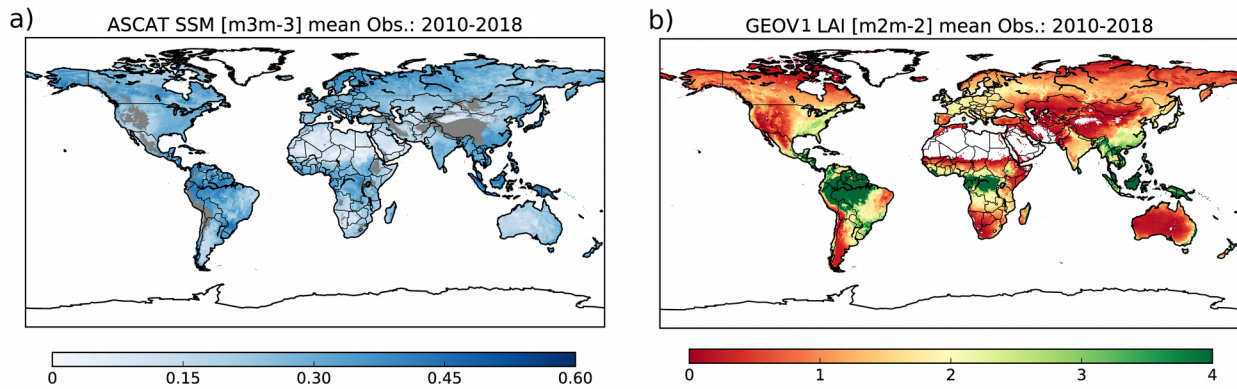


Figure 1: (a) Surface soil moisture (SSM) from the Copernicus Global Land Service (CGLS) for pixels with less than 15% of urban areas and with an elevation of less than 1500 m above sea level, (b) GEOV1 leaf area index (LAI) from CGLS, for pixels covered by more than 90 % of vegetation, averaged over 2010 to 2018. SSM is obtained after rescaling the ASCAT Soil Wetness Index (SWI) to the model climatology, grey areas on (a) represent filtered out data (see Section 2.3).

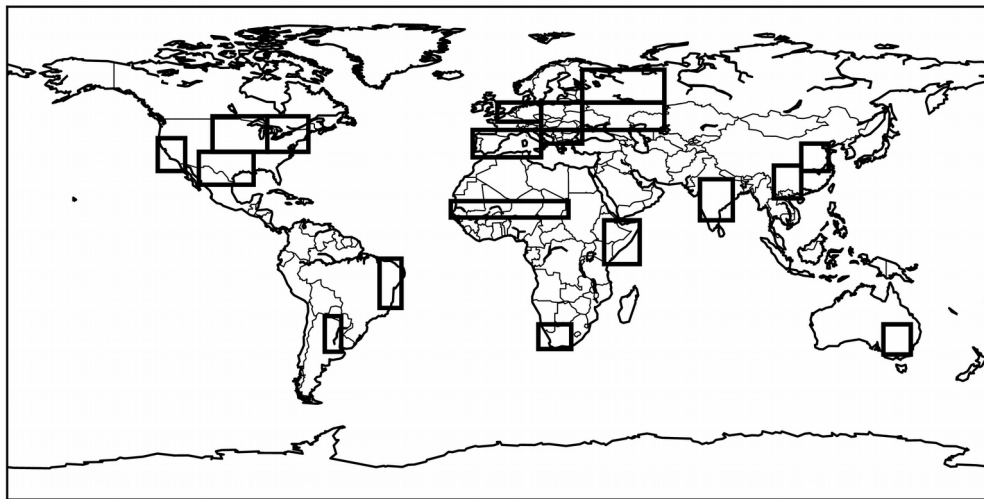


Figure 2: Selection of 19 regions across the globe known for being potential hot spots for droughts and heat waves, see section on experimental setup.

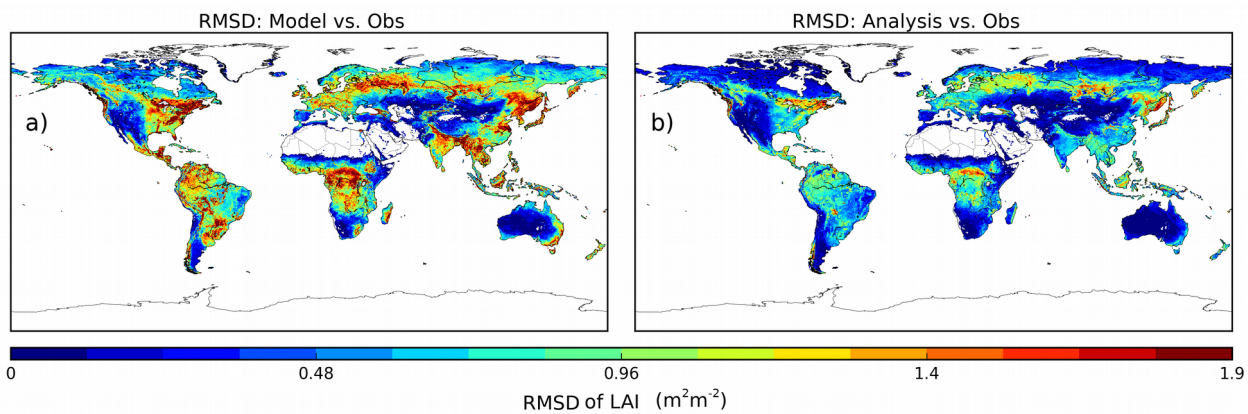


Figure 3: RMSD values between observed Leaf Area Index (LAI) and LDAS\_ERA5 (a) before assimilation and (b) after assimilation of surface soil moisture (SSM) and LAI.

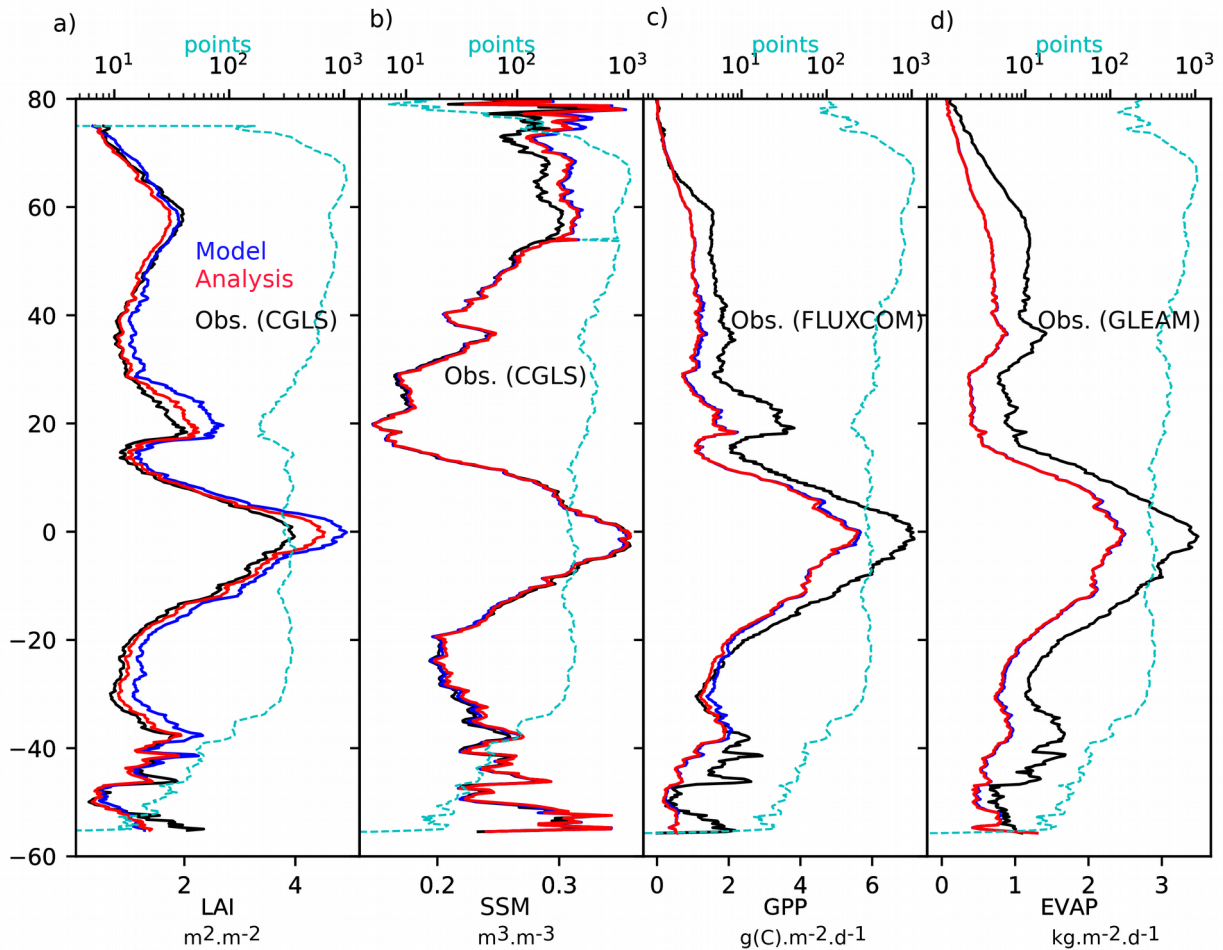


Figure 4: Latitudinal plots of (a) Leaf Area Index (LAI), (b) Surface Soil Moisture (SSM), (c) Gross Primary Production (GPP) and (d) Evapotranspiration for LDAS\_ERA5 before assimilation (Model, blue solid line) and after assimilation (Analysis, red solid line) as well as observations (black solid line). Cyan dashed line represents the number of points considered per latitudinal stripes of  $0.25^\circ$ .

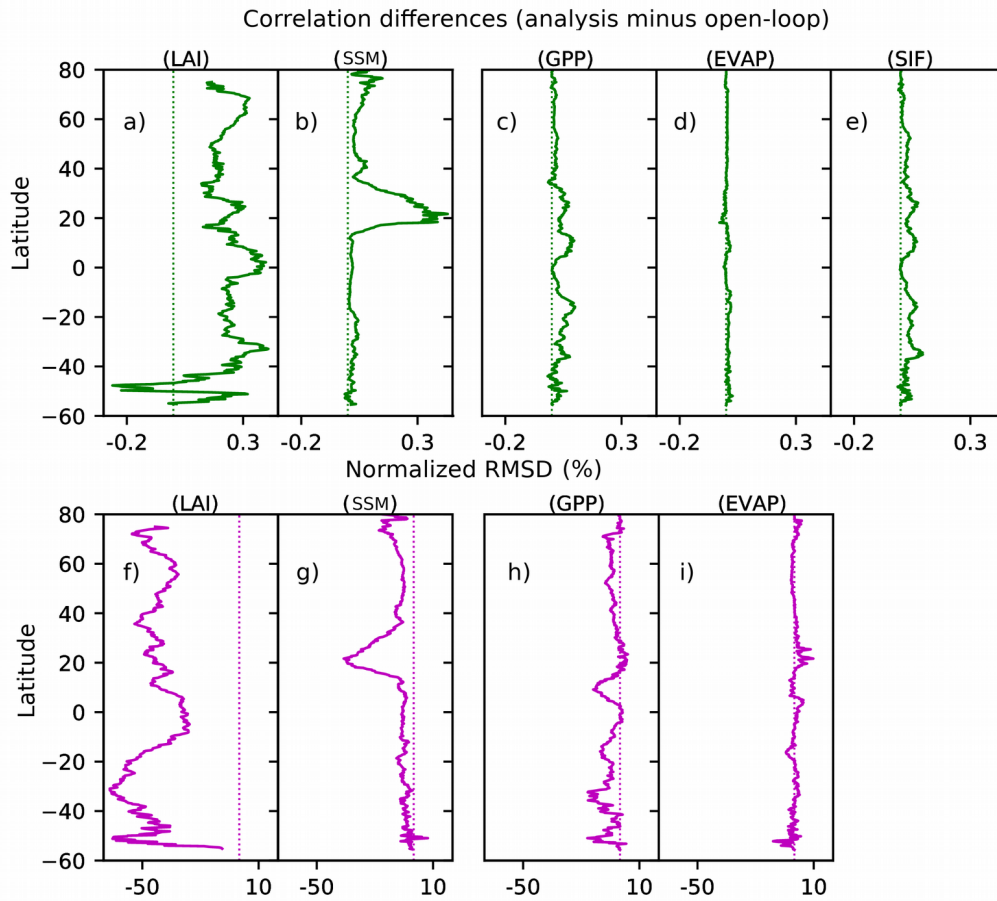


Figure 5: Latitudinal plots of score differences (analysis minus open-loop) for a) correlation, b) RMSD for Leaf Area Index (LAI), c) correlation, d) RMSD for Surface Soil Moisture (SSM 1-4 cm), e) correlation, f) normalized RMSD for Gross Primary Production (GPP), g) correlation, h) RMSD for evapotranspiration (EVAP) and I) correlation for Sun-Induced Fluorescence (SIF). Scores were computed based on monthly average over 2010-2018 for LAI and SSM, 2010-2013 for GPP, 2010-2016 for EVA and 2010-2015 for SIF. For SIF only differences in correlation are represented. Dashed lines represent the zero lines (equal scores for open-loop and analysis).

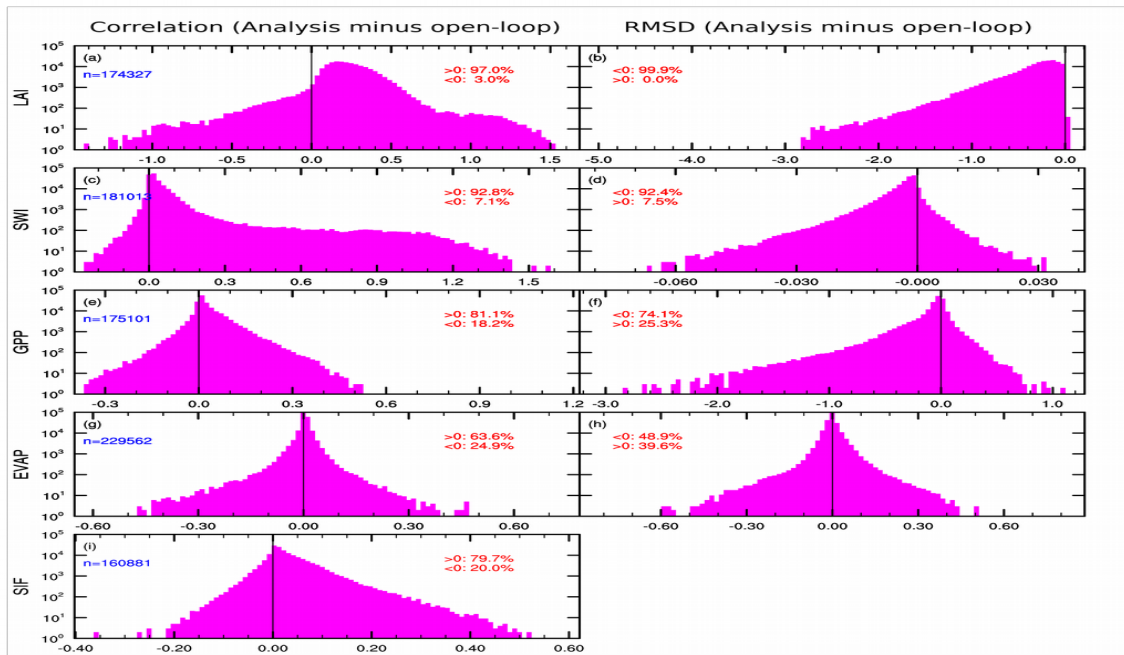


Figure 6: Histograms of score differences (correlation and RMSD, analysis minus open-loop) for a),b) Leaf Area Index (LAI), c),d) Surface Soil Moisture (SSM 1-4 cm), e),f) Gross Primary Production (GPP), g),h) evapotranspiration (EVAP) and i) Sun-Induced Fluorescence (SIF). Scores were computed based on monthly average over 2010-2018 for LAI and SSM, 2010-2013 for GPP, 2010-2016 for EVAP and 2010-2015 for SIF. For SIF only differences in correlation are represented. Number of available data (in blue) as well as the percentage of positive and negative values (in red) are reported. Note that for sake of clarity, the y-axis is logarithmic.

1150

1155



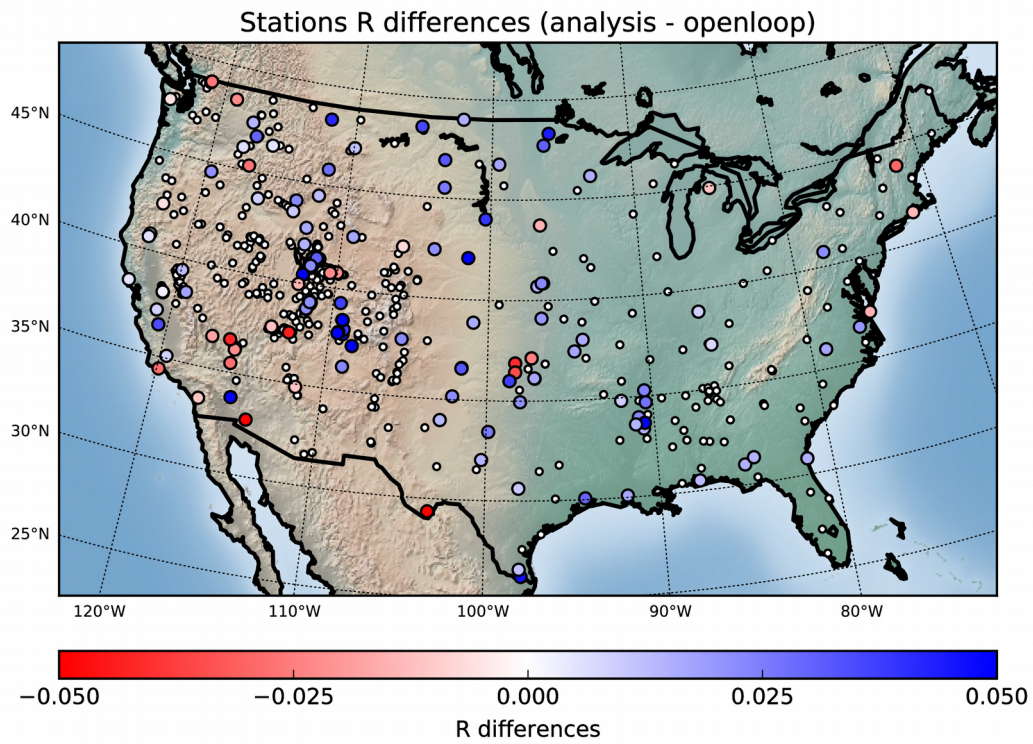


Figure 7: Map of correlations ( $R$ ) differences (analysis minus open-loop) for stations available over North America. Small dots represent stations where  $R$  differences are not significant (i.e. 95% confidence intervals are overlapping), large circles where differences are significant.

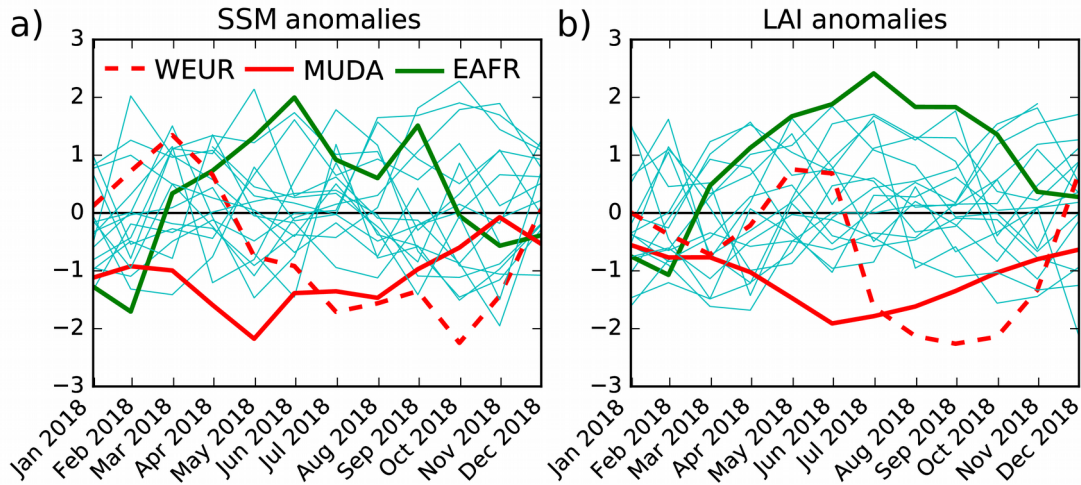


Figure 8: 2018 monthly anomalies scaled by standard deviation of analysed (a) Surface Soil Moisture (SSM, 1-4 cm) and (b) Leaf Area Index (LAI), with respect to 2010-2018, for the 19 regions presented in Table 1 and Figure 2. Solid red line, dashed red line and solid green line represent regions MUDA, WEUR and EAFR. Solid cyan line represent all other boxes (see Table 1 and Figure 2).

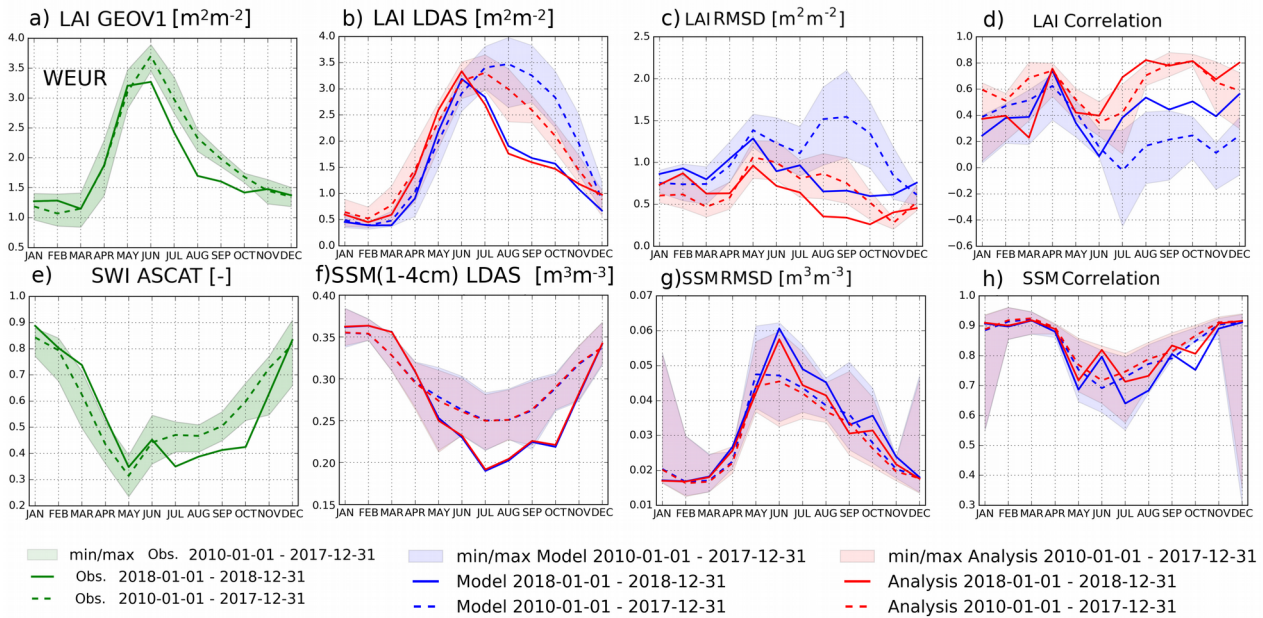


Figure 9: Seasonal cycles of a) observed Leaf Area Index (LAI) from the Copernicus Global Land Service (GEOV1, CGLS), b) LAI from the open-loop (in blue) and the analysis (in red), c) LAI RMSD values between either the open-loop or the analysis and the LAI GEOV1 for the Western Europe (WEUR) area (see Table I for geographical extent). d) same as (c) for correlation values. e) ASCAT Soil Wetness Index (SWI) from CGLS, f) g) and h) same as b), c) and d) for Surface Soil Moisture (SSM). Note that in g) and h) ASCAT SWI has been converted to SSM using the seasonal linear rescaling discussed in section 2.3 on assimilated Earth Observations dataset. For each panels dashed line represents the averaged over 2010-2017 along with the minimum and maximum values, the solid line is for year 2018.

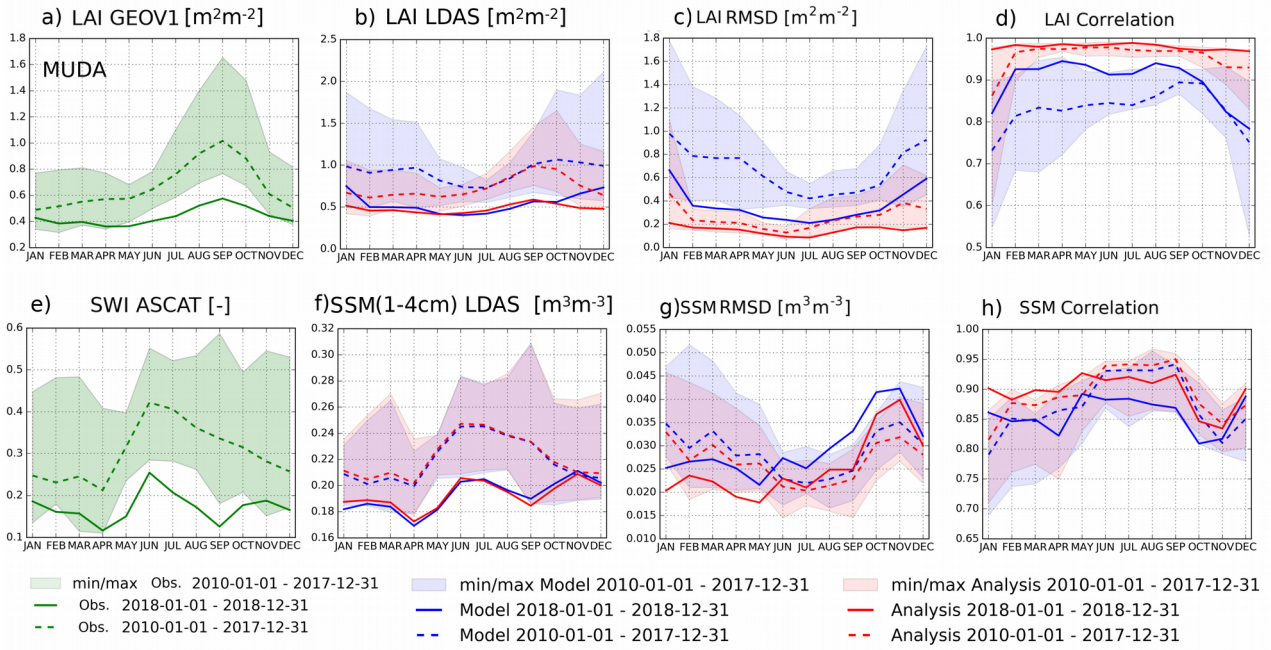


Figure 10: Same as Figure 9 for the Murray-Darling river (MUDA) area in south eastern Australia.

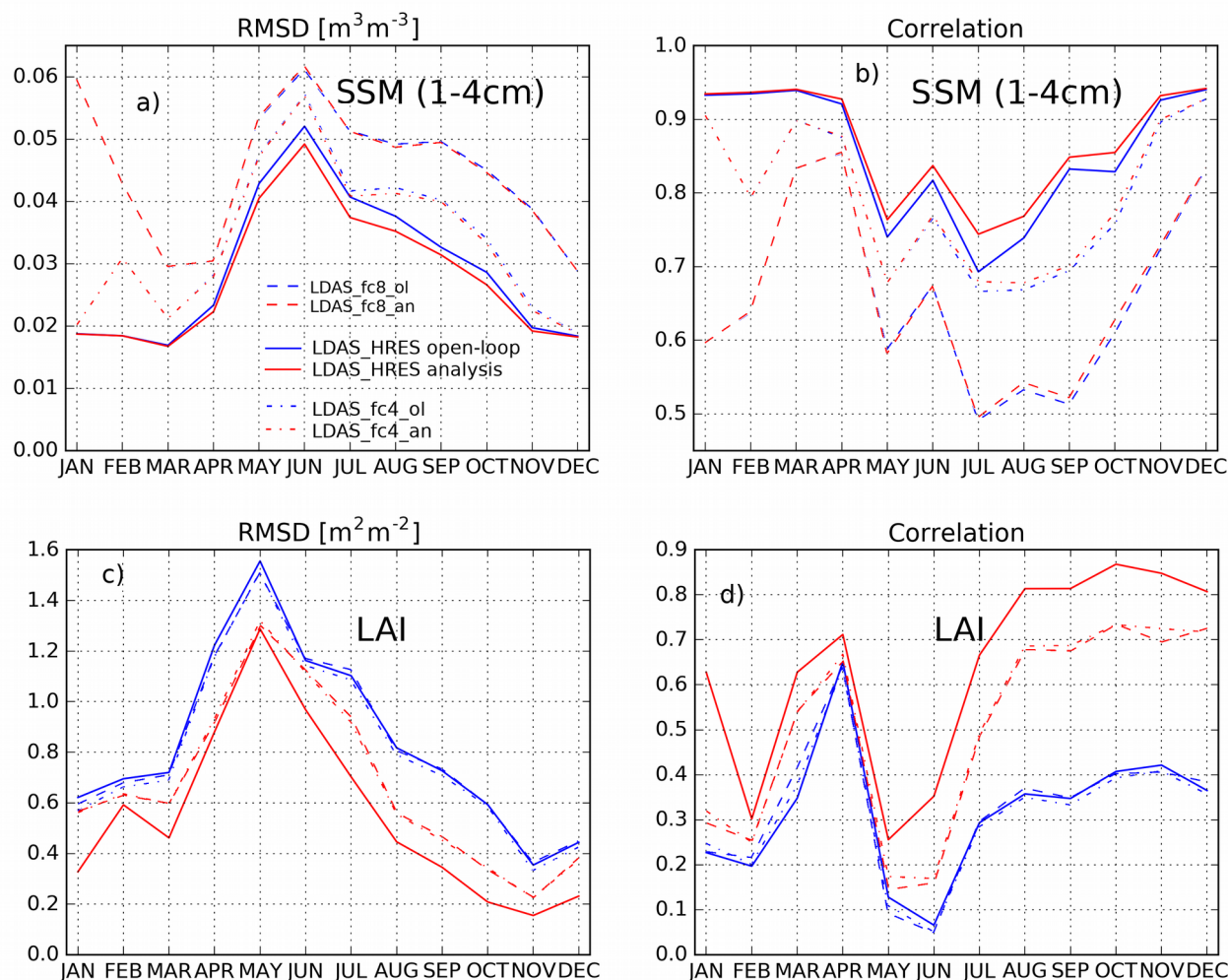


Figure 11: Upper panel, seasonal (a) root mean square differences (RMSD) and (b) correlation values between surface soil moisture (SSM) from the second layer of soil (1–4 cm) from the model forced by HRES (LDAS\_HRES, open-loop in blue solid line, analysis in red solid line) and ASCAT SSM estimates from the Copernicus Global Land Service project over 2017–2018 over the WEUR area. Scores between SSM from the second layer of soil of LDAS\_HRES 4-day (dashed/dotted blue – when initialised by the open-loop- and red – when initialised by the analysis- lines) and 8-day (dashed blue and red lines) forecasts and ASCAT SSM estimates are also reported. Lower panel (c) and (d), same as upper panel between modeled/analyzed Leaf Area index (LAI) and GEOV1 LAI estimates from the Copernicus Global Land Service project.

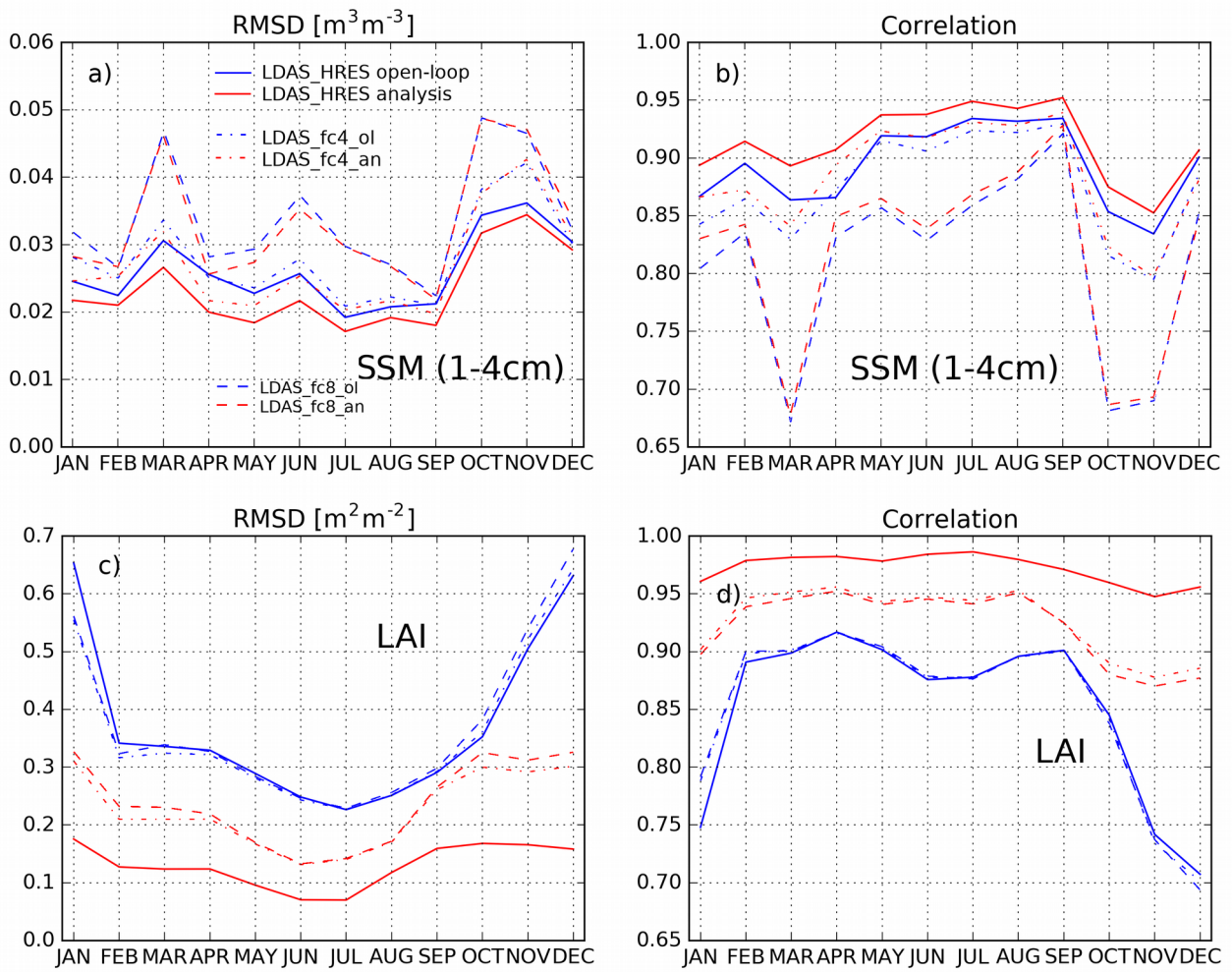


Figure 12: Same as Figure 11 for the Murray-Darling river (MUDA) area in southeastern Australia.

1175

1180

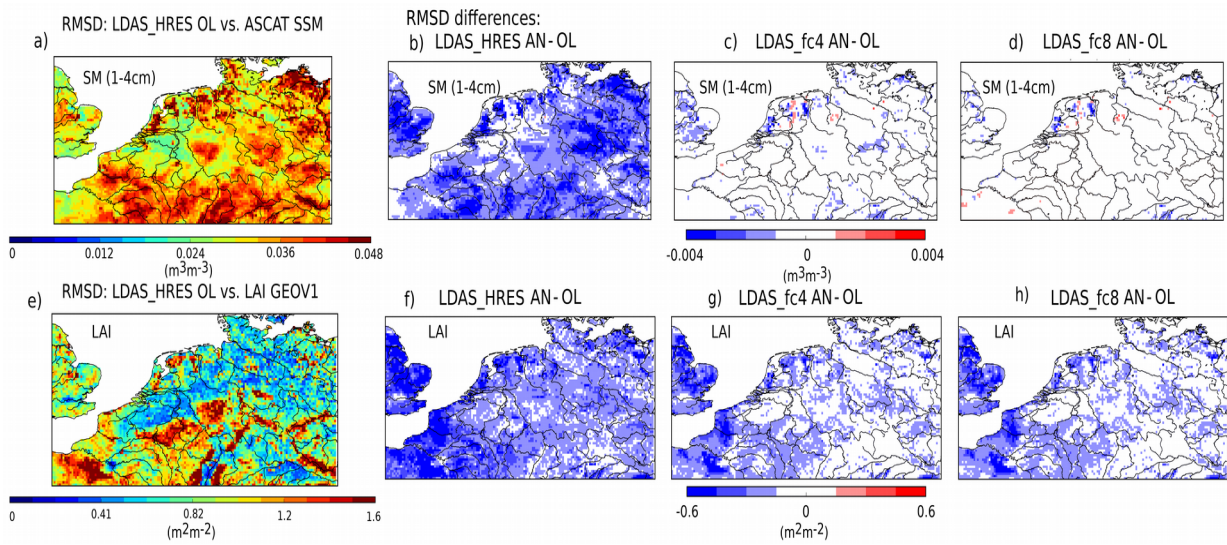


Figure 13: Top row, (a) RMSD values between LDAS\_HRES open-loop and ASCAT SSM estimates from the Copernicus Global Land Service (CGLS) over 2017-2018 for the WEUR domain, (b) RMSD differences between LDAS\_HRES analysis (open-loop) and ASCAT SSM. (c), (d) and (e) Same as (b) between LDAS\_fc4 initialised by the analysis (open-loop) and LDAS\_fc8. Bottom row, same as top row for Leaf Area Index (LAI) from the different experiments and LAI GEOV1.

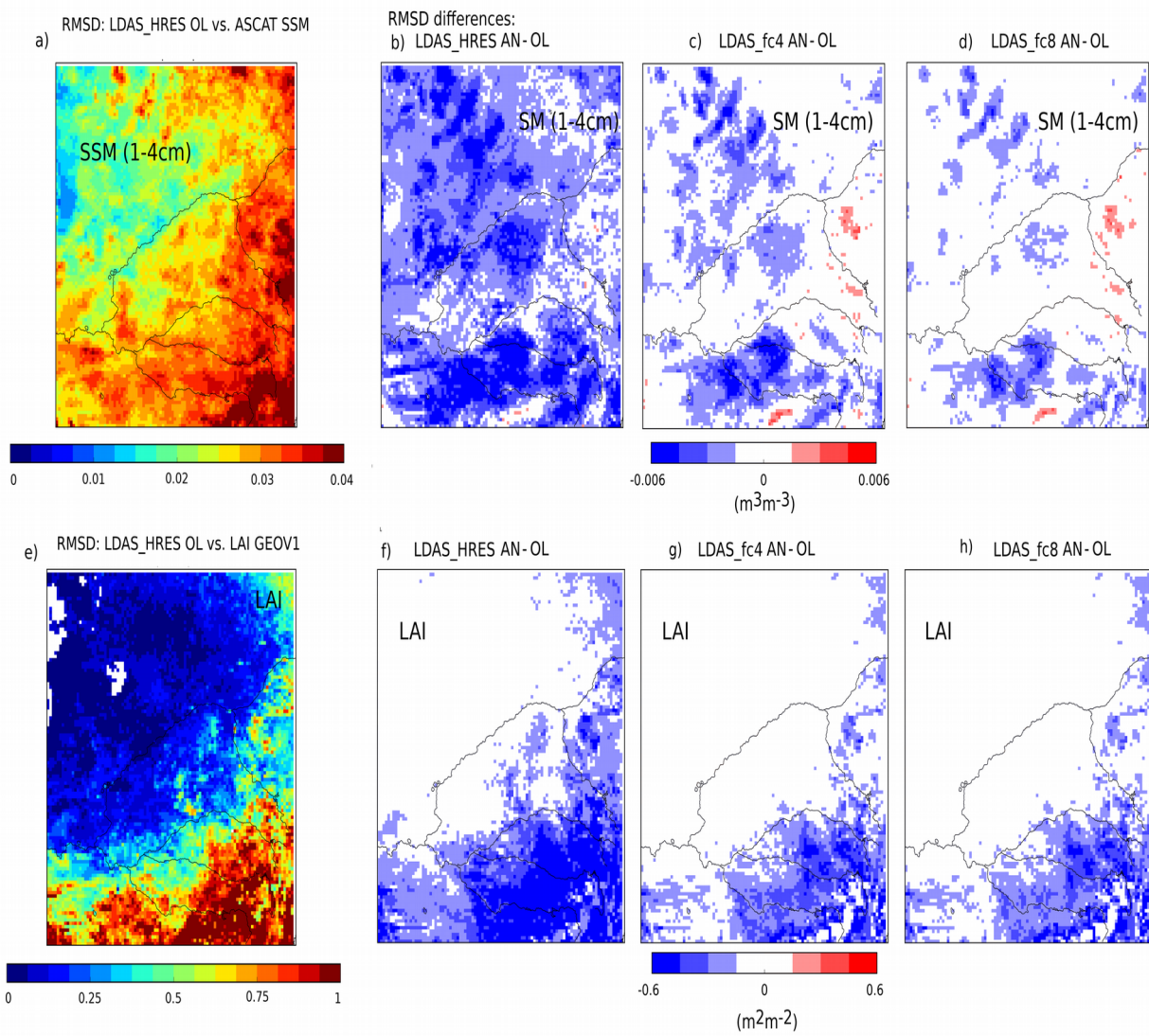


Figure 14: Same as Figure 13 or the Murray-Darling river (MUDA) area in south eastern Australia.



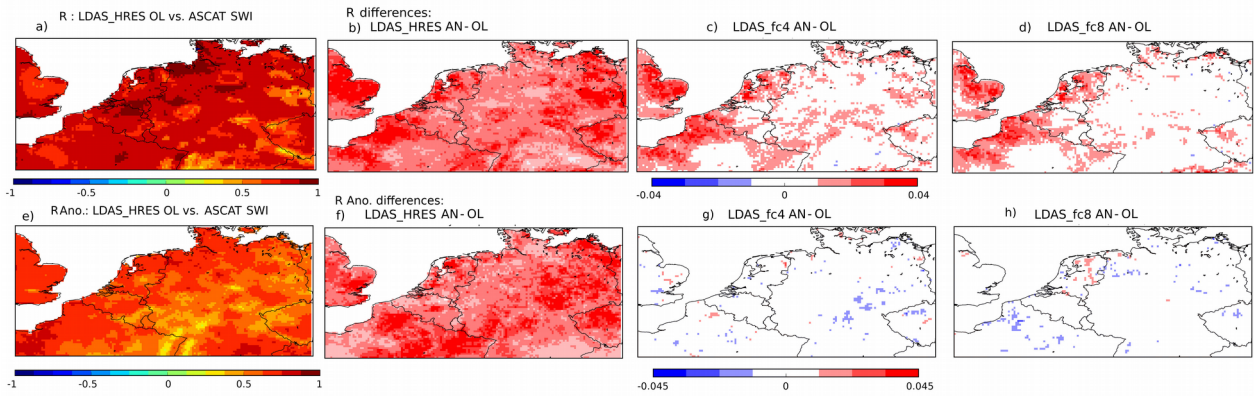


Figure 15: Top row, (a) R values between LDAS\_HRES open-loop and ASCAT SWI estimates from the Copernicus Global Land Service (CGLS) over 2017-2018 for the WEUR domain, (b) R differences between LDAS\_HRES analysis (open-loop) and ASCAT SWI. (c) and (d) same as (b) between LDAS\_fc4 initialised by the analysis (open-loop) and LDAS\_fc8. Bottom row, same as top row for R values based on anomaly time-series.

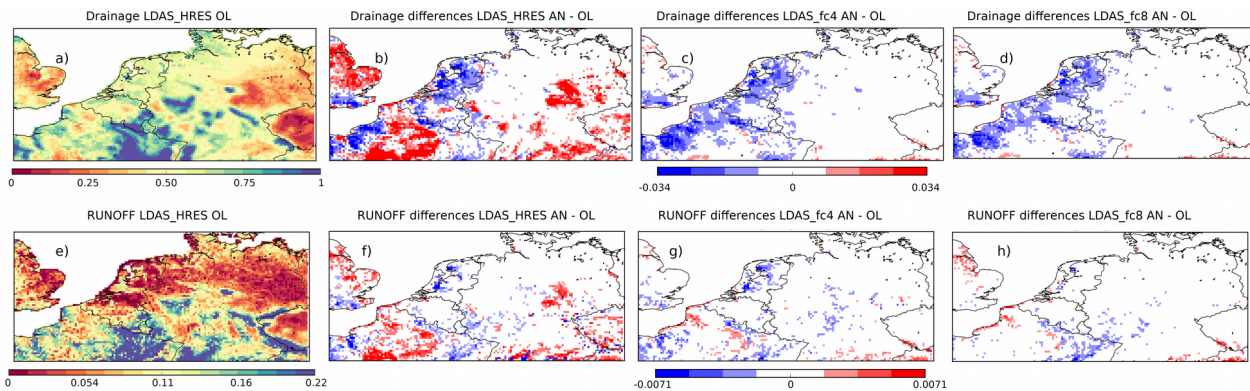


Figure 16: Top row, (a) drainage values for LDAS\_HRES open-loop over 2017-2018 for the WEUR domain, (b) drainage differences between LDAS\_HRES analysis and open-loop. (c), (d), same as (b) between LDAS\_fc4 initialised by the analysis and LDAS\_fc4 initialised by the open-loop, between LDAS\_fc8 initialised by the analysis and LDAS\_fc8 initialised by the open-loop. Bottom row, same as top row for runoff. Units are  $\text{kg.m}^{-2}.\text{day}^{-1}$